Mechanistic insights into c-di-GMP–dependent control of the biofilm regulator FleQ from Pseudomonas aeruginosa

Bruno y Matsuyama, Petya V. Krasteva, Claudine Baraquet, Caroline S Harwood, Holger Sondermann, Marcos V a S Navarro

Mechanistic insights into c-di-GMP–dependent control of the biofilm regulator FleQ from *Pseudomonas aeruginosa*

Bruno Y. Matsuyama[a,1], Petya V. Krasteva[b,c,1], Claudine Baraquet[d], Caroline S. Harwood[d,2], Holger Sondermann[c,2], and Marcos V. A. S. Navarro[a,2]

[a]Departamento de Física e Ciência Interdisciplinar, Instituto de Física de São Carlos, Universidade de São Paulo, São Carlos 13563-120, SP, Brazil; [b]Department of Structural Biology and Chemistry, Unité G5 Biologie Structurale de la Sécrétion Bactérienne and UMR 3528, CNRS, Institut Pasteur, 75015 Paris, France; [c]Department of Molecular Medicine, College of Veterinary Medicine, Cornell University, Ithaca, NY 14853; and [d]Department of Microbiology, University of Washington, Seattle, WA 98195

Contributed by Caroline S. Harwood, November 24, 2015 (sent for review September 29, 2015; reviewed by Martin Buck and Ann M. Stock)

Bacterial biofilm formation during chronic infections confers increased fitness, antibiotic tolerance, and cytotoxicity. In many pathogens, the transition from a planktonic lifestyle to collaborative, sessile biofilms represents a regulated process orchestrated by the intracellular second-messenger c-di-GMP. A main effector for c-di-GMP signaling in the opportunistic pathogen *Pseudomonas aeruginosa* is the transcription regulator FleQ. FleQ is a bacterial enhancer-binding protein (bEBP) with a central AAA+ ATPase σ^{54}-interaction domain, flanked by a C-terminal helix-turn-helix DNA-binding motif and a divergent N-terminal receiver domain. Together with a second ATPase, FleN, FleQ regulates the expression of flagellar and exopolysaccharide biosynthesis genes in response to cellular c-di-GMP. Here we report structural and functional data that reveal an unexpected mode of c-di-GMP recognition that is associated with major conformational rearrangements in FleQ. Crystal structures of FleQ's AAA+ ATPase domain in its apo-state or bound to ADP or ATP-γ-S show conformations reminiscent of the activated ring-shaped assemblies of other bEBPs. As revealed by the structure of c-di-GMP–complexed FleQ, the second messenger interacts with the AAA+ ATPase domain at a site distinct from the ATP binding pocket. c-di-GMP interaction leads to active site obstruction, hexameric ring destabilization, and discrete quaternary structure transitions. Solution and cell-based studies confirm coupling of the ATPase active site and c-di-GMP binding, as well as the functional significance of crystallographic interprotomer interfaces. Taken together, our data offer unprecedented insight into conserved regulatory mechanisms of gene expression under direct c-di-GMP control via FleQ and FleQ-like bEBPs.

enhancer binding protein | flagella | structure | gene expression

Bacterial adaptations to diverse environments, including human hosts, involve collaborative group behaviors, such as quorum sensing, swarming, and biofilm formation (1–5). In general, quorum-sensing during host tissue colonization is associated with virulence gene expression and acute-phase infections, whereas biofilm formation facilitates the development of chronic infections, evasion of host immune response, and increased tolerance to treatments (6). It is now well appreciated that these social behaviors result from highly regulated signal transduction processes, which in many bacteria are choreographed by the nucleotide-based second messenger c-di-GMP (7–9). Synthesized by GGDEF domain-containing diguanylate cyclases and hydrolyzed by EAL or HD-GYP domain-containing phosphodiesterases, c-di-GMP is sensed by a variety of protein- and RNA-based effectors to exert control at transcriptional, translational, and posttranslational levels (10, 11).

In *Pseudomonas aeruginosa*, an opportunistic pathogen that causes severe chronic infections in cystic fibrosis patients, burn victims, and other immunocompromised individuals, the transcription factor FleQ acts as a master regulator of flagellar motility and exopolysaccharide (EPS) secretion to mediate the transition between planktonic and biofilm lifestyles (12–14). FleQ contains an N-terminal REC receiver domain (Pa_FleQ^{REC}), a central AAA+ ATPase σ^{54}-interaction domain (Pa_FleQ^{AAA}), and a C-terminal helix-turn-helix DNA binding motif (Pa_FleQ^{HTH}) (Fig. 1*A*). FleQ shares significant homology and similarities in gene-expression regulation with members of the NtrC subfamily of bacterial enhancer binding proteins (bEBPs) (15).

Typically, bEBP with REC domains are regulated by phosphorylation via cognate histidine kinases, whereby transfer of a phosphoryl group from the kinase to the REC domain alters molecular interactions within or between bEBPs (16, 17). As a result, phosphorylated bEBPs, reorganized into ring-shape hexamers, bind ~150 bp upstream of the transcription start site, recruit the σ^{54}-RNAP–promoter complex, and initiate transcription in an ATPase-dependent manner (18–20). Despite similar domain architecture, however, FleQ appears to use a drastically different mechanism of regulation (13, 14, 21). FleQ

Significance

Pseudomonas aeruginosa, an opportunistic pathogen that can cause fatal chronic infections, relies on the intracellular second-messenger c-di-GMP to form robust multicellular biofilms during host tissue colonization. c-di-GMP is sensed directly by the transcription regulator FleQ, which inversely regulates flagellar motility and exopolysaccharide secretion to secure a planktonic to sessile life-form transition. FleQ belongs to the diverse family of AAA+ ATPase enhancer-binding proteins, but how its non-canonical function on transcriptional regulation is controlled by c-di-GMP remains enigmatic. Here, we report structural and functional data that identify an unusual mode of c-di-GMP recognition accompanied by a major quaternary structure reorganization. Our analyses offer a consensus to previous studies and unique insights into the mechanism of action of FleQ and FleQ-like proteins.

Author contributions: B.Y.M., P.V.K., C.B., C.S.H., H.S., and M.V.A.S.N. designed research; B.Y.M., P.V.K., C.B., and M.V.A.S.N. performed research; B.Y.M., P.V.K., C.B., C.S.H., H.S., and M.V.A.S.N. analyzed data; and P.V.K., H.S., and M.V.A.S.N. wrote the paper.

Reviewers: M.B., Imperial College London; and A.M.S., Center for Advanced Biotechnology and Medicine, University of Medicine and Dentistry of New Jersey-Robert Wood Johnson Medical School.

The authors declare no conflict of interest.

Freely available online through the PNAS open access option.

Data deposition: The atomic coordinates have been deposited in the Protein Data Bank, www.pdb.org (PDB ID codes 5EXP, 5EXS, 5EXT, and 5EXX).

[1]B.Y.M. and P.V.K. contributed equally to this work.

[2]To whom correspondence may be addressed. Email: csh5@uw.edu, hs293@cornell.edu, or mvasnavarro@ifsc.usp.br.

This article contains supporting information online at www.pnas.org/lookup/suppl/doi:10.1073/pnas.1523148113/-/DCSupplemental.

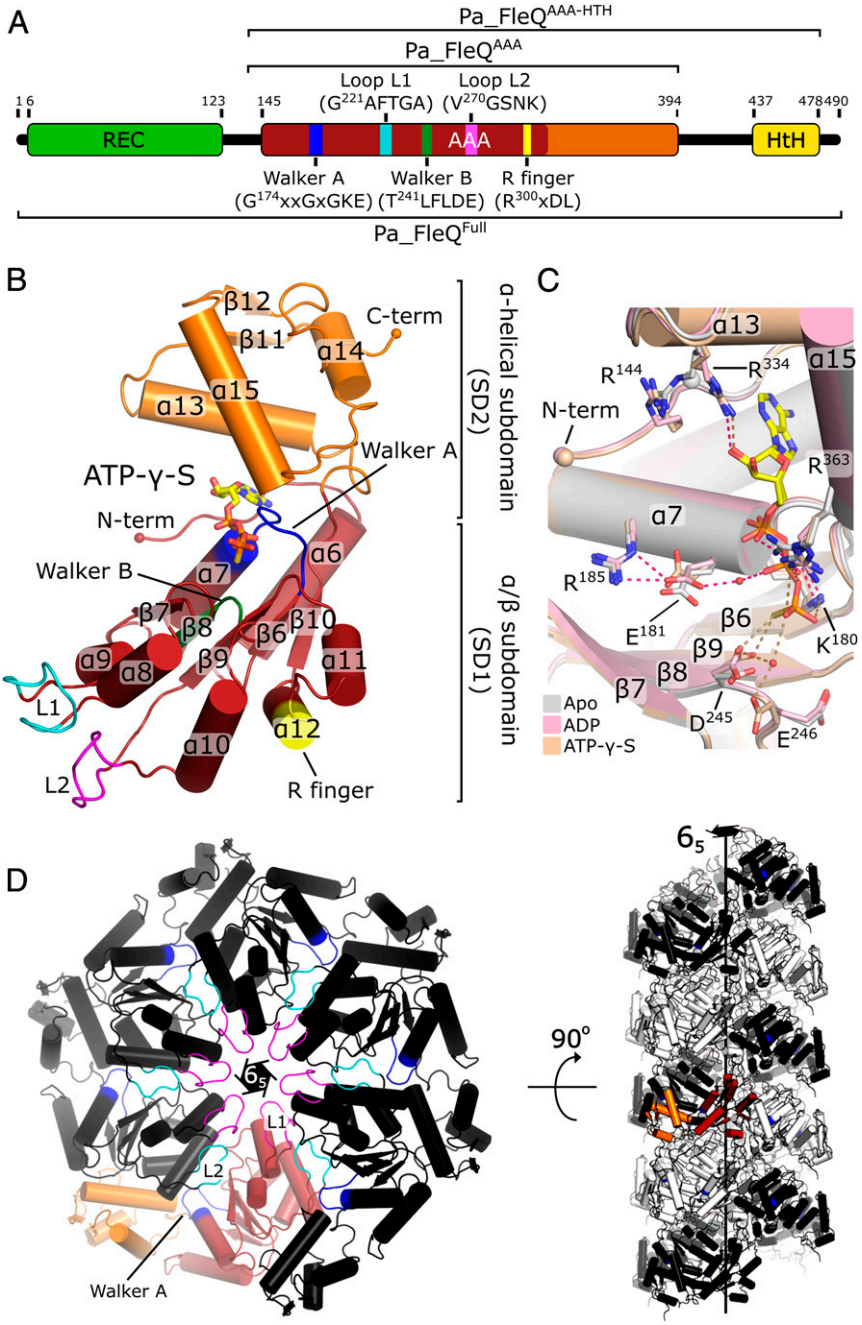

Fig. 1. Crystal structures of *P. aeruginosa* FleQ AAA+ domain reveal ring-shaped, hexameric assemblies. (*A*) Domain organization of FleQ. AAA+ functional motifs and bEBPs specific features discussed in the text are labeled. Full-length *P. aeruginosa* FleQ (Pa_FleQ^{Full}) and domain construct boundaries (Pa_FleQ^{AAA} and Pa_FleQ$^{AAA-HTH}$) used in this work are indicated. (*B*) Structure of an ATP-γ-S-bound Pa_FleQ^{AAA} protomer. Coloring of structural elements and AAA+ subdomains SD1 and SD2 is consistent with the diagram shown in *A*. (*C*) Superimposition of apo (gray), ADP-bound (pink), and ATP-γ-S-bound (orange) crystal structures. Red and brown dashed lines highlight interactions between FleQ residues and ADP or ATP-γ-S, respectively. (*D*) Crystallographic apo-Pa_FleQ^{AAA} hexamer assembly as viewed down the 6_5 fold axis. Symmetry generated protomers are colored in black. Walker A motif and σ^{54}-interacting loops L1 and L2 are shown in blue, magenta and cyan, respectively. (*Right*) An extended view of the crystal lattice in an orthogonal view. Intercalated black and white "open" hexamers appear as helical Pa_FleQ^{AAA} filaments running along the screw axis through the entire crystals.

lacks both a cognate sensor kinase and conserved REC domain residues that are crucial for phosphotransfer and phosphorylation-dependent conformational changes. Instead of relying on covalent modifications, its function depends on direct protein–protein interactions with FleN, a distinct ATPase that acts largely as a FleQ antagonist (22). Furthermore, at promoters of the flagellar biosynthesis gene cluster, FleQ not only binds to enhancer sequences upstream of the transcription start site—like classic bEBPs—but also at sites downstream from the transcription start sites (13, 23). In addition, and most relevant for this study, c-di-GMP directly binds to and regulates FleQ, altering target promoter activity (13, 14, 21).

C-di-GMP exerts distinct effects on FleQ's regulatory roles at the flagellar and EPS biosynthesis operons, underscoring the system's multifaceted role in biofilm formation (21). The dinucleotide dampens FleQ's ATPase activity and causes a modest but

significant down-regulation of flagellar gene expression (13, 14, 21). In contrast, FleQ acts as a repressor of Pel EPS expression in the absence of c-di-GMP. An increase of intracellular c-di-GMP levels through the action of diguanylate cyclases not only relieves FleQ-mediated gene repression, but it converts the protein into a potent transcription activator (13). Strikingly, gene expression activation under these conditions does not appear to require FleQ's intrinsic ATPase activity, is σ^{54}-independent, and likely proceeds through σ^{70} (21, 24). On both flagellar and *pel* promoters FleN further modulates FleQ-mediated gene regulation (14, 21). However, FleN's effect on the regulation of flagella expression and assembly is much more pronounced, with deletion of *P. aeruginosa fleN* leading to multiflagellated cells and only a small down-regulation in *pel* expression (14, 25).

How FleQ is able to exert such different effects and to sense different regulatory inputs at its target promoters has so far remained enigmatic. With regard to c-di-GMP signal recognition, at least two distinct modes of second-messenger binding in the context of FleQ's tertiary structure have been proposed (21, 26). It is unclear, however, how c-di-GMP recognition would affect the various aspects of the protein's higher-order regulatory mechanics. Here we present crystallographic data and solution-based structure-function analyses that reveal an unexpected mode of c-di-GMP regulation. In particular, we show that binding of the second messenger occurs at a composite site within the FleQ AAA+ domain and is accompanied by a major quaternary structure reorganization and allosteric ATPase inhibition. Our results reconcile previous modeling and functional studies (13, 14, 21, 26), and provide an integrated model for FleQ-dependent transcription regulation of genes involved in EPS production and secretion.

Results

Canonical, Ring-Shaped FleQ Hexamers Revealed by Crystal Structures of Its AAA+ Domain. The AAA+ ATPase domain of bEBPs couples ATP binding and hydrolysis to transcription complex remodeling (18). All bEBPs' functional features, including the specific σ^{54}-interaction loops—L1, which contains the signature GAFTGA motif (27), and L2—are conserved in FleQ (Fig. 1*A*). Purified, nucleotide-free Pa_FleQ^{AAA} (residues 137–394) crystallized in space group $P6_5$ and its structure was determined to 1.8 Å resolution by single-wavelength anomalous dispersion (SAD) phasing on iodide-derivatized crystals. Using the apo-structure as the search model, structures of Pa_FleQ^{AAA} cocrystallized with ADP or ATP-γ-S were solved by molecular replacement and refined to a resolution of 2.4 Å and 2.5 Å, respectively (Table S1). In these structures, Pa_FleQ^{AAA} adopts a canonical bilobal fold comprising a larger N-terminal α/β subdomain typical for P-loop NTPases (SD1) and an α-helical subdomain specific for AAA+ ATPases (SD2) (Fig. 1*B*) (20, 28). Apart from subtle changes caused by nucleotide coordination, the apo- and nucleotide-bound structures are virtually identical, with an all-atom rmsd lower than 0.6 Å in pairwise superpositions of protomers. Both ADP and ATP-γ-S interact with residues S^{176} and K^{180} from Walker A (G^{174}xxGxGKE), as well as with a conserved R^{363} from the so-called sensor II motif in subdomain SD2 (Fig. 1*C* and Fig. S1*D*) (28). Ribose sugar moieties are additionally coordinated by the SD2 residue R^{334}. In the ATP-γ-S–bound form, the γ-phosphate of the nucleotide is sensed by D^{245} and, indirectly, by E^{246} from the Walker B motif (T^{241}LFLDE) (Fig. 1*C* and Fig. S1*A*).

Although the asymmetric units of all three structures contain a single polypeptide chain, a view along the sixfold symmetry axes reveals protomer packing similar to the hexameric rings of activated canonical AAA+ proteins (Fig. 1*D*) (28). Rather than forming discrete oligomers, however, the protomers arrange in continuous spirals along the screw axes (Fig. 1*D*, *Right*). Interestingly, similar spiral arrangements are observed in the crystal packing of the isolated AAA+ domain of *Escherichia coli* PspF (Ec_PspF^{AAA}), a bEBP known to form discrete hexameric rings in solution (29). PspF ring oligomers are believed to undergo sequential hydrolysis where asymmetry in the intersubunit interactions confers cooperativity in nucleotide binding and catalysis (30). In addition, solution structural studies on ring hexamers of another nonhelical bEBP, NtrC1, revealed that one of the intersubunit interfaces is significantly less tight, which led to a mechanistic model where bEBP planar ring split is necessary to drive interactions with the σ^{54}-RNAP holoenzyme and ATP-dependent remodeling (31).

Because the formation of ring-shaped FleQ assemblies would only require subtle changes in the protomer-packing interfaces observed in the crystalline spirals, we continued by examining the actual oligomerization states of FleQ in solution. To this end, we visualized full-length FleQ (Pa_FleQ^{Full}) by negative-stain electron microscopy following gel filtration in the presence of the transition-state analog ADP-vanadate. Single-particle analysis of the micrographs failed to reveal any filamentous structures but showed discrete hexameric species that are consistent with canonical bEBP ring assembly rather than helical organization (Fig. S1*B*). Although these experiments were performed under saturating conditions of a single, nonhydrolyzable nucleotide species and more studies are necessary to examine potential conformational changes and asymmetry along the hydrolytic cycle, it is possible that the crystal packing of the isolated AAA+ domain from both Pa_FleQ and Ec_PspF in the form of open oligomers reflects a conserved mechanism for bEBP activation and function.

Molecular Determinants for c-di-GMP Recognition by FleQ's AAA+ Domain. In the presence of c-di-GMP, a purified AAA–HTH dual domain construct of *P. aeruginosa* FleQ (Pa_FleQ$^{AAA\text{-}HTH}$, residues 137–477) crystallized in space group $P6_322$ with a single protomer per asymmetric unit. Although the crystals were characterized by extremely high solvent content (~80%) and suboptimal anisotropic diffraction, the structure was determined by Se-SAD to 3.3 Å resolution with good refinement statistics (Table S1). The refined electron density map covers residues 138–393 and excludes the C-terminal HTH domain, likely because of flexibility in the loosely packed crystals and insignificant contribution to the X-ray diffraction data.

Two molecules of c-di-GMP bind in their preferred intercalated dimer conformation in a region between subdomains SD1 and SD2 that is different from the ATP-binding active site (Fig. 2*A* and Fig. S1*A*). An earlier modeling study on a FleQ homolog from *Vibrio cholerae*, FlrA, suggested that residues corresponding to R^{144} and R^{185} of *P. aeruginosa* FleQ constitute a conserved c-di-GMP binding site at the REC and AAA+ domain interface (26), which was recently confirmed by another modeling-based study (32). The Pa_FleQ$^{AAA\text{-}HTH}$–c-di-GMP cocrystal structure not only confirms the importance of these residues for c-di-GMP recognition, but also reveals a composite binding site with contributions from three key motifs within a single FleQ protomer (Fig. 2*A*). *Cis*-acting residues include: a proximal c-di-GMP-binding switch located at the N-terminus of the AAA+ domain that is composed of the LFR^{144}S motif (R-switch); residues R^{185} and N^{186} in helix α7 of subdomain SD1 (post-Walker A); and finally, a distal c-di-GMP-binding motif comprising the ExxxR^{334} sequence in helix α13 of subdomain SD2 (Fig. 2 *A* and *B*). Isothermal titration calorimetry confirms both the stoichiometry of binding (~2:1 for c-di-GMP:Pa_FleQ^{Full} with an apparent affinity constant K_d of ~4.1 μM) and the role of conserved arginine residues in ligand coordination (Fig. S2 *A* and *B*).

A systematic sequence analysis of bEBPs revealed a higher degree of conservation of c-di-GMP binding motifs (R-switch, post-Walker A and ExxxR consensus motifs) within FleQ homologs (Fig. 2*B*). This group includes the c-di-GMP–responsive regulator FlrA from *V. cholerae*, for which the importance of R^{135}

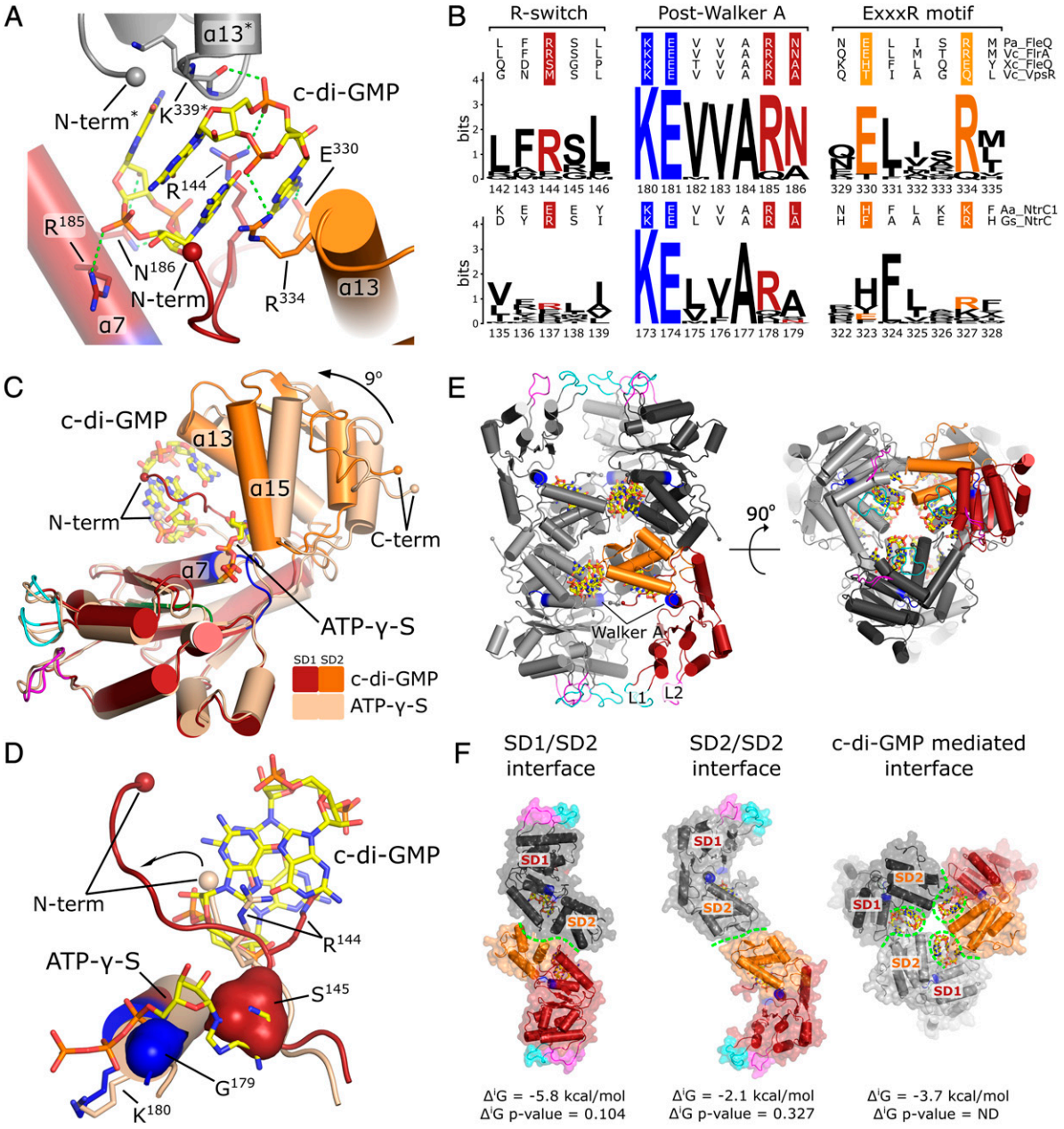

Fig. 2. Crystal structure of c-di-GMP–bound Pa_FleQ$^{AAA\text{-}HTH}$ reveals major oligomeric rearrangements. (*A*) Close-up view of the c-di-GMP binding site. Interactions (green dashes) between intercalated c-di-GMP dimer and conserved dinucleotide binding residues R^{144}, R^{185}, N^{186}, E^{330}, and R^{334} are shown. A crystal symmetry-related protomer that completes the c-di-GMP binding site is shown in gray. Labels that refer to the symmetric protomer contain asterisks. (*B*) Sequence conservation of the c-di-GMP binding site. Sequence logo representations of multisequence alignment for FleQ and NtrC1 homologs cover the three motifs involved in c-di-GMP recognition within the AAA+ domain. bEBPs sequences without a regulatory N-terminal domain or with REC, GAF or FleQ-like N-terminal domains were selected from the RP55 database with HMMER (60) and logos were generated with Skylign (61). Representative sequences are shown on top of the logos: *P. aeruginosa* FleQ (Pa_FleQ); *V. cholerae* FlrA (Vc_FlrA); *X. citri* FleQ (Xc_FleQ); *V. cholerae* VpsR (Vc_VpsR); *A. aeolicus* (Aa_NtrC1); *Geobacter sulfurreducens* NtrC (Gs_NtrC). (*C*) Comparison between c-di-GMP and ATP-γ-S–bound structures. Superposition of the respective SD1 domains reveals a 9° rigid body rotation (black arrow) of the SD2 subdomain relative to the SD1 domain upon c-di-GMP binding. The c-di-GMP–bound Pa_FleQ$^{AAA\text{-}HTH}$ structure is colored as in Fig. 1; bound nucleotides are shown as sticks (yellow carbon atoms). (*D*) The N-terminal segment of FleQ's AAA+ domain partially occupies the ATP site in the c-di-GMP–bound structure. Solid surface representation of S^{145}'s side chain and G^{179}'s main chain indicate steric hindrance at the ATP binding site caused by the conformational change induced by c-di-GMP. (*E*) Assembly composed of head-to-head dimers of c-di-GMP–stabilized trimers in two orthogonal views. Pa_FleQ$^{AAA\text{-}HTH}$ crystal symmetry-related protomers are colored in different shades of gray. (*F*) Protein–protein interfaces within the c-di-GMP–bound Pa_FleQ$^{AAA\text{-}HTH}$ dimer-of-trimers. The assembly involves head-to-head SD1/SD2 (*Left*) and SD2/SD2 (*Center*) interfaces and a c-di-GMP–mediated (*Right*) interface. Dissociation energies (Δ^iG) and corresponding interaction-specificities (Δ^iG *P* value) for each individual interface (green dashes) were calculated with the PISA server (36).

and R^{176} (corresponding to FleQ R^{144} and R^{185}, respectively) for c-di-GMP binding has been determined experimentally (26). In particular, the coconservation of all three c-di-GMP-binding motifs, and especially their arginine residues, is striking (Fig. 2*B*). Consistent with this notion, isothermal titration calorimetry (ITC) experiments with a FleQ homolog from *Xanthomonas*

citri (XAC1967), which contains divergent c-di-GMP binding motifs (Fig. 2*B*), failed to show c-di-GMP binding (Fig. S2*C*). On the other hand, co-occurring arginine residues important for c-di-GMP binding were found in several bEBPs with different N-terminal regulatory domains (Fig. 2*B*, Table 1, Fig. S3, and Table S2). Of 4,632 bEBPs mined from a representative proteome database (33), ∼3% presented conserved c-di-GMP binding residues, suggesting that c-di-GMP regulation of bEBP-mediated transcription may be more widely used than previously anticipated, potentially participating in other cellular processes beyond flagellar regulation and EPS secretion (Fig. 2*B* and Table 1). Additionally, the absence of the aforementioned conserved c-di-GMP binding motifs in the atypical bEBP VpsR from *V. cholerae* (34) and in AAA+ ATPases involved in multiple bacterial secretion systems (35), all shown to bind to c-di-GMP, further suggest that bacterial AAA+ domains may represent ubiquitous targets for c-di-GMP, yet with distinct binding sites.

Consequences of c-di-GMP Binding on FleQ's Tertiary and Quaternary Structure. Compared with apo, ADP-, and ATP-γ-S–bound Pa_FleQ^{AAA} structures, the conformation of the c-di-GMP-bound AAA+ ATPase σ^{54}-interaction domain reveals novel and unexpected features at both the tertiary and quaternary structure levels. Protomer superposition using subdomain SD1 as the reference reveals a 9° rigid body movement of subdomain SD2 to a more compact, c-di-GMP–stabilized conformation relative to the apo-, ADP-, and ATP-γ-S–bound structures (Fig. 2*C*). It has been proposed previously that c-di-GMP competes with ATP for binding to the AAA+ ATPase domain active site based on the fact that c-di-GMP competitively inhibits ATP hydrolysis and that a Walker A disruptive mutation (FleQ K^{180}A) abolishes c-di-GMP binding to FleQ (21). However, this model is at first sight inconsistent with the crystallographic analysis. Superposition of the c-di-GMP– and ATP-γ-S–bound Pa_FleQ^{AAA} structures reconciles the apparent contradictions by revealing that c-di-GMP binding shifts the N terminus of the AAA+ domain into the ATP-binding pocket (Fig. 2*D*), thus acting as an allosteric inhibitor of the protein's hydrolytic activity and, by extension, of σ^{54}-dependent transcription activation. Importantly, in the context of the full-length protein, such an N-terminal movement in the FleQ AAA+ domain would cause a drastic repositioning of the preceding FleQ^{REC} module, possibly contributing to the disruption of the active-state hexameric ring (Fig. S1*C*). Finally, residue K^{180} in the Walker A motif occupies a pivotal location between the two AAA+ subdomains and plays a significant role in stabilizing interprotomer interaction within Pa_FleQ^{AAA} hexameric rings (Fig. S1*D*). A mutation in this position could interfere with both c-di-GMP–mediated AAA+ interdomain movement and oligomeric assembly.

The structural organization of the c-di-GMP binding pocket provides further evidence for negative coupling of this site with the ATPase active site. The highly conserved residues R^{144}, R^{185}, and R^{334} are not only directly involved in c-di-GMP coordination (Fig. 2*A* and Fig. S2), but also directly or indirectly stabilize ATP binding, as observed in the ADP and ATP-γ-S–complexed Pa_FleQ^{AAA} crystal structures (Fig. 1*C*). In particular, residue R^{334} is in direct contact with the ribose moiety of ATP, while also stabilizing the N-terminal AAA+ domain segment through π-stacking interactions with R^{144} (Fig. 1*C*). Similarly, residue R^{185} forms a salt bridge with the Walker A residue E^{181}, and might also sense nucleotide binding (Fig. 1*C*). All these specific interactions important for ATP binding and hydrolysis are disrupted in the c-di-GMP–bound state.

The most striking feature of the c-di-GMP–bound structure, however, is the profound reorganization of crystallographic interfaces, which suggests dramatic quaternary structure reorganization upon allosteric second-messenger recognition. The observed c-di-GMP–mediated subdomain movement and N-terminal restructuring appear incompatible with the maintenance of canonical bEBP ring hexamers. Indeed, symmetry-related protomers arrange into a distinct hexameric species where c-di-GMP–stabilized trimers dimerize in a head-to-head fashion ("dimer-of-trimers") (Fig. 2*E*). Dissociation energy analyses of protein-protein and c-di-GMP–protein interfaces (SD1/SD2, SD2/SD2, and c-di-GMP–mediated interfaces) suggest biological relevance for this unique oligomeric arrangement (Fig. 2*F*) (36). Within the trimeric assembly mediated by c-di-GMP, a total buried surface area of about 1,400 Å^2 yields a gain of −14.4 kcal/mol in solvation energy. The hexamer formed by SD1/SD2 and SD2/SD2 subdomain pairings further occludes ∼4,300 Å^2 of surface area, with a total gain in solvation energy of −23.7 kcal/mol. To our knowledge, such architecture is unprecedented for bEBP family members and underscores the unique mechanism of FleQ regulation and function.

C-di-GMP Drives FleQ Oligomeric Reorganization in Solution. External signal stimuli, such as ligand binding (ATP or promoter DNA) and protein phosphorylation at the REC domain, usually trigger the switch of inactive bEBP dimers to ring-like activated hexamers (17, 19, 37). In this regard, FleQ behavior deviates once again from canonical bEBPs, by being able to spontaneously hexamerize in solution (21). In addition, although the N-terminal domain of FleQ shares sequence homology with canonical REC domains, it lacks both sequence conservation at the putative phosphorylation site and a cognate histidine kinase (12), making regulatory phosphorylation unlikely.

To evaluate the role of ligand binding on FleQ oligomerization in solution, we captured discrete oligomeric species through chemical cross-linking with the amine-reactive compound ethylene glycol bis-(succinimidyl succinate) (EGS). In agreement with previous results (21), wild-type full-length FleQ (Pa_FleQ^{Full}) showed a dimeric fraction as well as discrete higher-order species (mostly tetramers and hexamers), regardless of the absence or presence of ATP-γ-S (Fig. 3). A cross-linking time-course revealed a gradual accumulation of the higher oligomeric species, suggesting an equilibrium between FleQ oligomers in solution (Fig. 3*A*). Most notably, however, addition of c-di-GMP stalled FleQ oligomerization beyond a dimeric species, regardless of ATP-γ-S availability (Fig. 3*B*). The striking effect of c-di-GMP on FleQ's oligomeric assembly mirrors the dinucleotide's effect on FleQ's protease sensitivity (21), and corroborates c-di-GMP–driven quaternary structure changes inferred from the crystal structures (Figs. 1 and 2).

Similar cross-linking experiments using FleQ constructs lacking the REC domain, Pa_FleQ^{AAA} and Pa_FleQ$^{AAA\text{-}HTH}$, showed less pronounced effects (Fig. S4). In particular, oligomerization of Pa_FleQ^{AAA} was severely compromised, with the protein migrating mostly as a monomer, independent of nucleotide (Fig. S4*A*). This result is consistent with a recent report that dimerization of the noncanonical REC domains is critical for FleQ oligomerization and function (32). Inclusion of the C-terminal HTH domain restored in-solution dimerization partially (Fig. S4*B*). Addition of c-di-GMP

Table 1. Sequences of bEBPs presenting conserved c-di-GMP binding motifs

N-terminal regulatory domain	Total of sequences in RP55 database*	Sequences with conserved c-di-GMP binding motifs†
FleQ‡	90	67 (74.4%)
GAF	238	5 (2.1%)
—	1257	8 (0.6%)
REC	3047	62 (2.0%)

*Sequences of FleQ and NtrC (REC) homologs used for the Logo generation in Fig. 2*B*.
†All three motifs conserved; see Table S2 for accession numbers.
‡FleQ refers to the N-terminal degenerated REC domain.

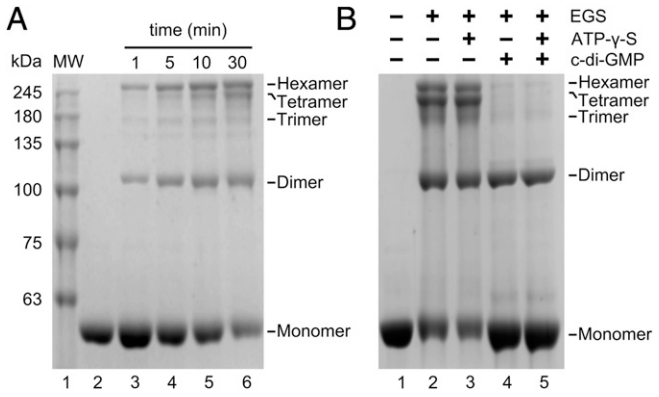

Fig. 3. Cross-linking analysis of full-length FleQ oligomerization in solution. SDS/PAGE analyses of PA_FleQ^{Full} protein (10 μM) incubated with or without the primary amine-specific cross-linker EGS are shown. (*A*) FleQ cross-linking time course in the absence of nucleotides. The sample in lane 2 was not incubated with EGS. All other samples were incubated with EGS (250 μM). (*B*) Effects of nucleotides on FleQ cross-linking. Addition of nucleotides (100 μM) is indicated above the gel. Where indicated, samples were incubated for 30 min at room temperature in the presence of EGS (1 mM). Migration pattern of probable oligomeric species are indicated on the right of each gel.

stablized higher-order oligomers of Pa_FleQ^{AAA} (and to a lesser extent Pa_FleQ$^{AAA\text{-}HTH}$) including trimers and hexamers, consistent with a change in quartenary structure and our crystallographic analyses. These results mirror studies on trunctation mutants of other bEBPs, which revealed oligomerization properties and functional activities distinct from their full-length counterparts. For example, removal of the N-terminal regulatory domain of *Salmonella enterica* serovar Typhimurium NtrC and *Aquifex aeolicus* NtrC1 inhibits or promotes, respectively, the formation of activated oligomeric ring assemblies (19, 20).

Taken together, our data indicate that c-di-GMP antagonizes different FleQ oligomeric assemblies, in accordance with our structural analyzes. The cross-linking studies not only indicate a crucial role of the REC domain for spontaneous FleQ oligomerization but also suggest that hexamer formation may be a prerequisite of c-di-GMP binding.

Functional Analysis of Interface-Disruptive FleQ Variants Confirm Biological Significance of Crystallographic Oligomers. We next designed a set of single-point mutations to confirm the role of crystallographic protein–protein and protein–ligand interfaces on full-length FleQ oligomerization, as well as on ATPase activity and c-di-GMP binding. Mutant I^{374}E was designed to perturb formation of bEBP canonical ring-like hexamers apparent in the apo-, ADP-, and ATP-γ-S–bound Pa_FleQ^{AAA} structures; mutants R^{185}E, N^{186}A, E^{330}A and R^{334}E were designed to directly inhibit c-di-GMP binding; and two additional mutations were chosen to disrupt the SD1/SD2 (T^{149}E) or SD2/SD2 (V^{380}E) interfaces observed in the c-di-GMP–bound Pa_FleQ$^{AAA\text{-}HTH}$ structure (Fig. 4*A*). The proper folding and preserved stability of all mutants introduced in the full-length protein were verified by circular dichroism experiments of thermal denaturation (Fig. S5*A*).

In the absence of c-di-GMP, higher molecular weight oligomers beyond dimers were severely disrupted only with the I^{374}E mutant, consistent with our structure-based prediction (Fig. 4*B*). Mutants with disrupted c-di-GMP binding pocket (R^{185}E and R^{334}E) retained wild-type–like oligomerization patterns, but were impaired in c-di-GMP's antagonistic effect on assembly (Fig. 4*B* and Fig. S5*B*). Mutations designed to disrupt the interfaces SD1/SD2 and SD2/SD2 observed in the c-di-GMP–bound structure, T^{149}E and V^{380}E, respectively, maintained FleQ's propensity to form hexamers, rendering the protein apparently insensititve to c-di-GMP (Fig. 4*B*, lanes 5–6, and Fig. S4*B*). Hence, destabilization of the crystallographically observed dimer-of-trimers appears to have a positive effect on the stability of the canonical bEBP hexamer. Similar to wild-type FleQ, ATP-γ-S did not alter the oligomerization propensities of any of the mutants (Fig. S5*B*).

Based on the fact that FleQ is an active ATPase that is primarily dimeric in solution, it has been proposed previously that the dimers are the catalytically active conformation (21). As we show here, however, FleQ samples higher-order oligomeric conformations in solution, including hexameric rings (Fig. 3 and Fig. S1*B*), and its AAA+ domain crystallizes in a conformation consistent with the active-state ring hexamers of canonical bEBPs (Fig. 1*D*). These data prompted us to dissect the role of oligomerization on the protein's catalytic activity. In ATPase activity assays, we observed a severe reduction in the ATP hydrolysis rate with the I^{374}E mutant (Fig. 4*C*). Because the cross-linking indicates a defect in hexamer formation while dimerization is preserved in this mutant, these data assert the hexamer as the catalytically active conformation.

The ATPase activity data also confirm conformational coupling between the c-di-GMP– and ATP-binding pockets: disruption of the conserved R^{185} and R^{334} residues abolishes not only c-di-GMP binding, but also ATPase activity (Fig. 4*C* and Fig. S2*B*), in line with their structural role in active-site stabilization (Fig. 1*C*). Mutants designed to disrupt crystallographic, c-di-GMP–mediated dimer-of-trimers, T^{149}E and V^{380}E, have preserved and even enhanced ATPase activity (7.5- and 1.5-fold increase over wild-type for T^{149}E and V^{380}E, respectively) (Fig. 4*C*). Analysis of the known inhibitory effect of c-di-GMP on FleQ's ATPase activity (21) revealed that although the V^{380}E mutation reduces c-di-GMP sensitivity only slightly, the high activity of the T^{149}E mutant remains unaffected (Fig. 4*D*).

To evaluate the impact of SD1/SD2 or canonical ring interface perturbations on c-di-GMP binding, we performed ITC experiments with FleQ variants T^{149}E and I^{374}E, respectively. Under the same experimental conditions used for wild-type Pa_FleQ^{Full}, ITC results with both mutants revealed a severe reduction of heat released during the titration (Fig. 4*E*), indicating that disruptive mutations at both oligomeric interfaces observed in the distinct crystallographic hexamers (ring-shaped or dimer-of-trimers) (Figs. 1*D* and 2*E*) negatively affects c-di-GMP binding.

FleQ Oligomeric Reorganization Triggered by c-di-GMP Is Compatible with Its Repressor-to-Activator Functional Transition on EPS Gene Expression. FleQ recognizes two sites (FleQ boxes 1 and 2), separated by 34 bp, in the *pelA* promoter region (Fig. S6) (13). Previous reports showed that FleQ, stabilized by FleN and ATP/ADP, binds to both sites simultaneously, promoting a kink in the DNA and thus repressing gene expression (13). C-di-GMP binding to FleQ relieves the DNA distortion and activates gene expression without affecting the apparent protein occupancy on DNA (13, 14). In a mutant strain with a *fleN* deletion, FleQ still acts as an ATP-independent repressor of *pel* expression and increased c-di-GMP levels induce FleQ-mediated *pel* expression, albeit at a reduced level (14). Hence, the *ΔfleN* genetic background offers a unique possibility to examine directly the role of FleQ's quaternary structure on *pel* transcriptional repression and activation. To evaluate the physiological role of the structural transition observed in vitro on transcriptional regulation via FleQ, we tested the effect of the various FleQ variants on *pel* operon expression in vivo.

Wild-type or mutant FleQ was expressed from a single-copy under its native promoter in a *ΔfleN* background. Elevated c-di-GMP levels were achieved by the coexpression of the active diguanylate cyclase YfiN/TpbB/PA1120 (38, 39). In line with previous results, *pel* expression was markedly enhanced upon YfiN

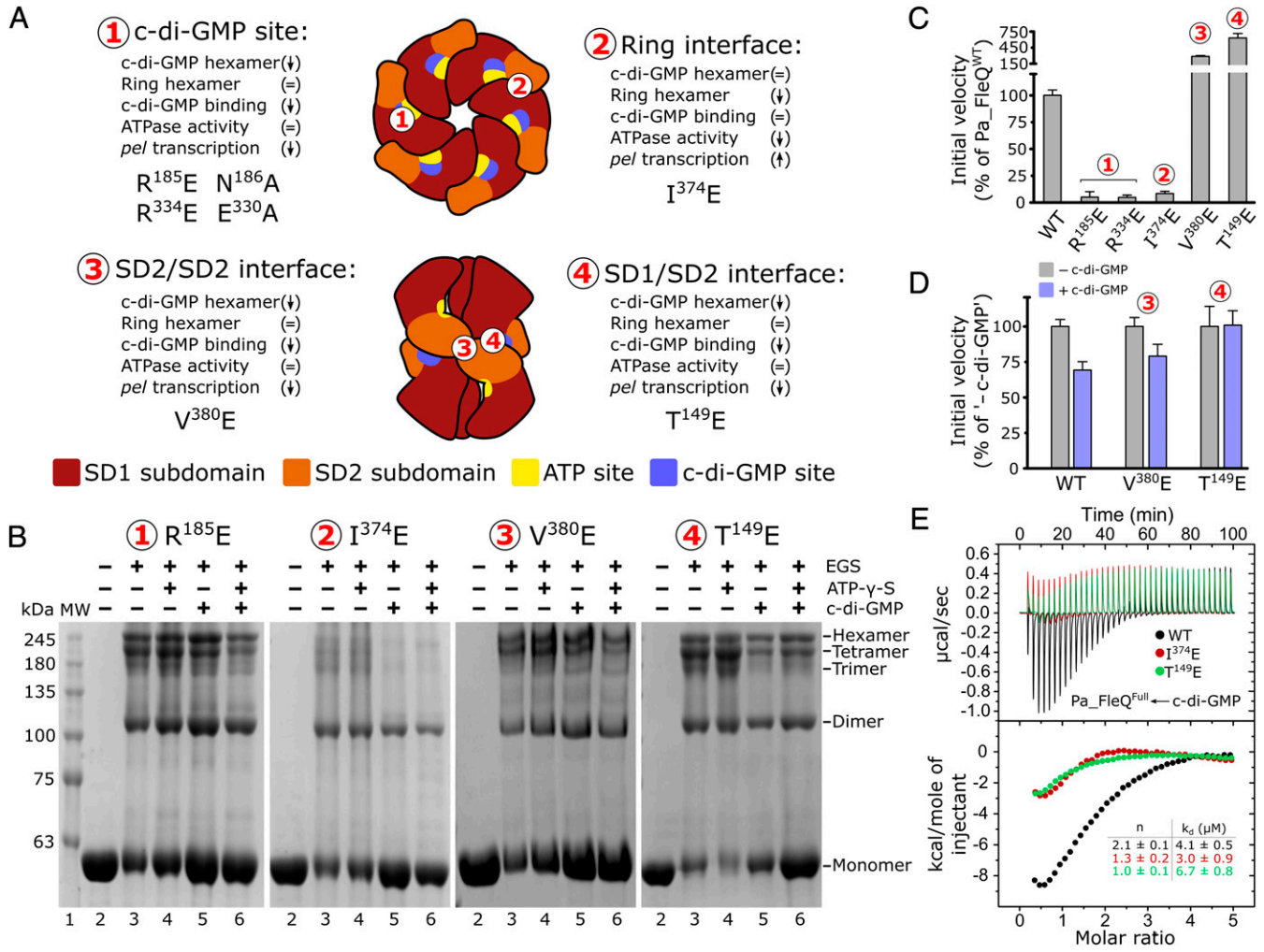

Fig. 4. Functional analyses of structure-guided Pa_FleQ^{Full} mutants. (*A*) Overview of site-directed mutants and predicted outcome. The diagram shows the position of each mutant on a cartoon of the hexameric ring or the dimer-of-trimers assembly. Predicted outcomes on FleQ function are indicated, distinguishing between indifferent (=), positive (↑), and negative (↓). (*B*) Cross-linking analysis. Mutant proteins were treated as described in Fig. 3, which shows the corresponding data for wild-type protein. (*C*) ATPase activity. Initial velocity of Pa_FleQ^{Full} variant-catalyzed ATP hydrolysis is shown expressed as percentage of wild-type Pa_FleQ^{Full} activity (1 μM protein; 1 mM ATP). The error bars represent SDs of triplicates. (*D*) c-di-GMP effect on ATP hydrolysis. ATPase activity of selected FleQ variants preincubated with c-di-GMP (50 μM). The error bars represent SDs of triplicates. (*E*) c-di-GMP binding. ITC of Pa_FleQ^{Full} T^{149}E and I^{374}E. The heat change upon ligand binding (μcal/s) and fitted curves to the integrated heat peaks are shown in the top and bottom titration curves, respectively. Binding stoichiometry and apparent dissociation constants are indicated in the table inset.

coexpression with wild-type FleQ, indicating c-di-GMP–dependent transcription derepression and activation (Fig. 5*A*) (14). As expected, both promoter repression and YfiN effects were abolished in a *fleQ* deletion strain. Consistent with the structural and biochemical data, c-di-GMP binding mutants (R^{185}E, N^{186}A, E^{330}A, and R^{334}E) exhibited markedly repressed *pel* transcription similar to wild-type *fleQ*, but remained virtually unchanged upon YfiN overexpression (Fig. 5*A*). The mutant T^{149}E, predicted to disrupt the c-di-GMP–stablized crystallographic dimer-of-trimers, also yielded repressed *pel* transcription, independent of c-di-GMP. Consistent with its residual c-di-GMP sensitivity as demonstrated by the ATPase data, mutant V^{380}E showed a somewhat derepressed *pel* transcription upon coexpression of a diguanylate cyclase (Figs. 4 and 5*A*). Notably, the I^{374}E mutant was characterized by constitutively active *pel* expression, suggesting that hexameric ring formation is required for repression of the operon (Fig. 5*A*).

Taken together, the expression data in mutant genetic backgrounds corroborate the structural and biochemical results, indicating an equilibrium between ATPase-active, *pel* repressive hexamers, and other less-functional oligomeric species. However, ATPase activity is not required for FleQ's function as a transcriptional repressor at the *pel* operon. C-di-GMP appears to exert its stimulatory effect on *pel* expression on FleQ variants that retain their ability to form hexamers and display an intact dinucleotide binding site (e.g., wild-type and V^{380}E).

Discussion

In response to specific stimuli, canonical bEBPs from the large AAA+ family of σ^{54}-dependent transcription regulators couple ATP hydrolysis to promoter-RNAP initiation complex remodeling to control associated gene expression (15). Although unusual, some bacterial activators, such as *Pseudomonas putida* PhhR, *E. coli* TyrR, *Rhodobacter capsulatus* HupR, and *Myxococcus xanthus* HsfA share similar domain architecture with bEBPs, but activate the σ^{70}-RNAP holoenzyme instead of the σ^{54}-associated transcriptional machinery (40–42). *P. aeruginosa* FleQ combines both canonical bEBP σ^{54}- and atypical σ^{70}-dependent transcriptional mechanisms to inversely control flagellar motility and EPS production, respectively (13, 14, 21). Significantly, FleQ is also regulated by the bacterial

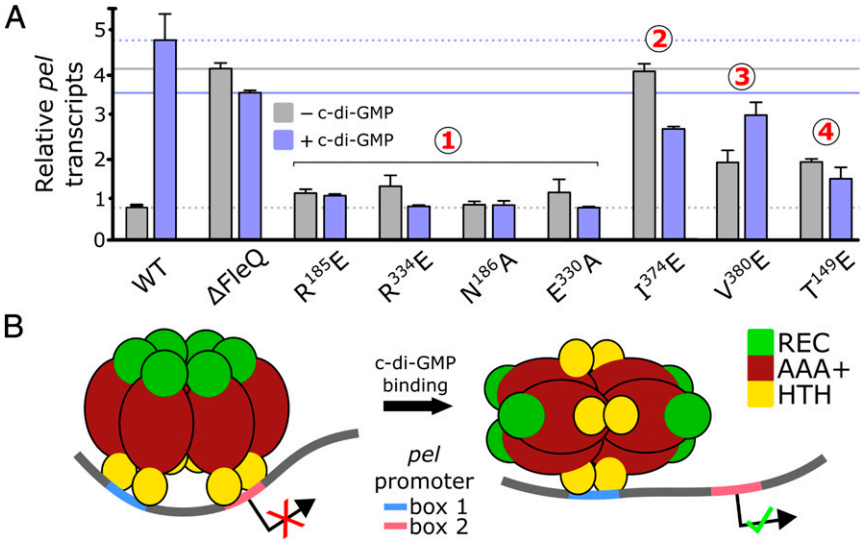

Fig. 5. Effect of FleQ site-directed mutants on *pel* transcriptional control. (*A*) Expression data. Relative *pelA* transcript levels in strains of *P. aeruginosa* PAO1 that lack *fleN* (designated WT) or *fleN* and *fleQ* (designated/Δ*fleQ*) were quantified by RT-PCR. Structure-guided mutations in the *fleQ* gene were expressed from a single copy introduced into the Δ*fleN*/Δ*fleQ* genome. Transcripts were measured with (blue; + c-di-GMP) or without (gray; – c-di-GMP) expression of the diguanylate cyclase PA1120 from a plasmid. Unbroken (Δ*fleN*/Δ*fleQ*) and dashed (Δ*fleN*; wild-type FleQ) colored lines indicate reference *pel* expression levels at low and high c-di-GMP conditions. (*B*) Molecular model of FleQ-mediated *pel* transcription. The diagram depicts a model incorporating our structural and functional data, focusing on the events in the absence of FleN and ATP.

second messenger dinucleotide, c-di-GMP (14). To gain molecular insight into the mechanism of c-di-GMP–dependent regulation of *P. aeruginosa* EPS gene expression by FleQ, we determined structures of its AAA+ domain in the apo-state and bound to ADP, ATP-γ-S, and c-di-GMP. Analyses of these structures, combined with in vitro and in vivo functional studies, revealed that *P. aeruginosa* FleQ undergoes a major conformational change upon c-di-GMP binding, concomitant with oligomeric rearrangement.

On one hand, the results presented here indicate a hexameric FleQ as the functional *pel* transcription repressor and as the target of c-di-GMP, because destablilization of the canonical AAA+ ring interfaces reduces c-di-GMP binding to FleQ (mutant $I^{374}E$) (Figs. 4 and 5 and Fig. S1*C*). On the other hand, perturbations at the unique interfaces that support the crystallographic, c-di-GMP–bound FleQ dimer-of-trimers (e.g., mutants $T^{149}E$ and $V^{380}E$) not only render the protein variants insensitive to c-di-GMP, but also stabilize highly ATPase-active FleQ oligomers (Fig. 4). This finding may suggest that different FleQ oligomers with distinct properties exist in equilibrium (Fig. 4).

In light of our results and previous studies on the regulation of EPS gene expression, we propose that canonical bEBP ring-like FleQ hexamers (Fig. 1*D* and Fig. S1*B*) bind both boxes 1 and 2 at the *pelA* promoter, which inhibits transcription initiation (Fig. 5*B*). Apparently, FleQ's function as a *pel* repressor in the absence of the cofactor FleN does not require its ATPase activity, but depends on the protein's ability to form higher-order oligomers, in particular hexameric rings (Figs. 4 and 5). The hexamer-to-DNA interaction model is also compatible with the promoter bending observed previously (Fig. S6) (13). The current hypothesis is that association of ATP-bound FleN to the FleQ:DNA complex is necessary to increase DNA curvature in vitro and that the FleQ–FleN interaction cooperatively enhances c-di-GMP binding (13, 21), consistent with full activation of FleQ-c-di-GMP–mediated *pel* transcription requiring FleN (14). In analogy, the repression of σ^{70}-dependent *tyrR* expression by the atypical bEBP TyrR from *E. coli* occurs via binding of tyrosine-stabilized hexamers to two adjacent sites at the promoter DNA (14, 43–46), suggesting that the mechanism described here might be a recurrent form of transcriptional repression by atypical bEBPs.

In the presence of c-di-GMP, FleQ undergoes conformational changes and alters its quaternary structure (Figs. 2 and 3), which may decrease affinity for at least some promoter interaction sites, thus relieving DNA bending and activating gene transcription (Fig. 5 and Fig. S6) (14). bEBPs interact with σ^{54} via two loops, L1 and L2. However, in our structures, these loops are accessible in the c-di-GMP–stabilized oligomer and not subject to conformational changes (Fig. 2*C*), suggesting a mode of transcriptional activation different from canonical bEBPs (18). The lack of conservation or absence of σ^{54}-interacting loops in other σ^{70}-dependent bEBP, such as *E. coli* TyrR and *P. putida* PhhR, respectively, argues further against their role in the direct activation of *pel* expression (40, 46).

Our data explain the molecular mechanism underlying c-di-GMP regulation of FleQ's functions as repressor and activator of *pel* expression, which likely depends on σ^{70} and is only moderately affected by the cofactor ATPase FleN. Future studies will focus on the roles of the N-terminal regulatory domains upstream of the AAA+ core and accessory proteins such as FleN in the context of FleQ's oligomeric states, and in particular on the regulation of flagellar gene regulation. The latter process requires FleQ's ATPase activity and σ^{54}, distinct from the mechanism described here, and presumably mirrors those of canonical bEBPs. How σ^{54}- and ATPase-dependent processes are coordinated with σ^{70}-dependent but ATPase-independent regulation at different promoters remains an open question.

Materials and Methods

Recombinant DNA Techniques. DNA manipulations were carried out using standard molecular biology techniques. For protein expression and purification, the ORFs of full-length and truncated FleQ variants were PCR-amplified from *P. aeuruginosa* PA14 genomic DNA and cloned in-frame into a modified pET28a expression plasmid (Novagen). Expression yields recombinant proteins with an N-terminal hexahistidine-SUMO moiety that can be liberated by incubation with yeast Ulp1 protease. FleQ point mutants were generated using QuikChange site-directed mutagenesis kit (Agilent), following the manufacturer's instructions. Successful mutagenesis was confirmed by DNA sequencing.

Protein Expression and Purification. Native and selenomethionine-derivatized proteins were overexpressed in *E. coli* BL21 (DE3) (Novagen) or T7 Crystal Express (New England Biolabs) cells, respectively. For the expression of native proteins, cells were grown at 37 °C in lysogeny broth (LB) medium supplemented with 50 μg/mL kanamycin. At a cell density corresponding to an absorbance of 0.6 at 600 nm (OD_{600}), the temperature was reduced to 20 °C and protein production was induced with 1 mM IPTG. Selenomethionine-derivatized proteins were produced in cells grown in M9 minimal medium supplemented with 50 μg/mL kanamycin, 1 μg/mL thiamine, 1 μg/mL biotin, 0.4% glucose, and 40 μg/mL of each of the 20 amino acids with selenomethionine substituting for methionine. Protein expression was induced at an OD_{600} of 0.4. After overnight expression, the cells were harvested by centrifugation, resuspended in resuspension buffer (25 mM Tris·HCl pH 8.0 and 300 mM NaCl) and lysed by sonication. Cell debris was removed by centrifugation and the cleared lysates were loaded onto TALON metal affinity resin (Clontech). The matrix was washed with 20 column volumes (CV) of resuspension buffer, followed by elution of bound proteins with elution buffer (25 mM Tris·HCl pH 8.0, 300 mM NaCl, and 500 mM imidazole). The eluted fractions were buffer-exchanged into resuspension buffer and incubated with Ulp1 protease at 4 °C overnight. Cleaved His_6-SUMO tags and uncut protein was removed via TALON metal affinity chromatography, and the cleaved target proteins were recovered in the flow-through. Purified protein was subjected to size exclusion chromatography on a HiLoad 16/600 Superdex 75 column (GE Healthcare) in gel-filtration buffer (25 mM Tris·HCl pH 8.0 and 300 mM NaCl). Purity of the proteins was analyzed by SDS/PAGE.

Circular Dichroism Spectroscopy. Circular dichroism measurements were performed using a J-720 (JASCO) spectroscope. Initial spectra of Pa_FleQ^{Full} and mutants (5 μM in 20 mM phosphate buffer, pH 7.2; 0.1-cm light-path quartz cuvette) were obtained by averaging 16 scans over a wavelength range of 200–260 nm. To eliminate background effects, buffer contributions were subtracted in all measurements. Spectra were transformed to molar ellipticity (θ). Thermal denaturation analyses were carried out by measuring the ellipticity at 220 nm over a temperature range from 10 °C to 95 °C, at a constant heating rate of 10 °C/h. The fraction of denatured protein was calculated from the relationship $(\theta_n - \theta_{obs})/(\theta_n - \theta_d)$, where θ_{obs} is the ellipticity of the sample at a particular temperature and θ_d and θ_n are the values of ellipticity characteristic of the denatured and native state, respectively.

Crystallization, Data Collection, and Structure Determination. Initial crystallization screens were conducted via sitting-drop vapor diffusion using commercial crystallization screens. Pa_FleQ^{AAA} crystallized at 18 °C against a solution of 0.1 M Bis-Tris pH 6.5, 0.2 M ammonium sulfate, and 25% (wt/vol) PEG3350. For crystallization of ADP- and ATP-γ-S–bound Pa_FleQ^{AAA}, the protein was preincubated with a fivefold molar excess of nucleotide for 2 h at 10 °C. Crystals of c-di-GMP–bound $Pa\_FleQ^{AAA\text{-}HTH}$ were obtained at 4 °C in the presence of 1 mM c-di-GMP in the drop and 0.05 M Bis-Tris pH 6.5, 30% (vol/vol) pentaerythritol ethoxylate (15/4 EO/OH), and 0.05 M ammonium sulfate in the mother liquor.

For data collection, crystals were soaked in mother liquor supplemented with cryo-protectants [up to 25% (wt/vol) xylitol or ethylene glycol] and flash-frozen in liquid nitrogen. Diffraction data were collected using either a Cu-rotating anode X-ray source (Pa_FleQ^{AAA}–ATP-γ-S) or synchrotron beamlines (beamline MX2 of the Laboratório Nacional de Luz Síncrotron, Campinas, Brazil, for apo-Pa_FleQ^{AAA} and Pa_FleQ^{AAA}-ADP; beamline A1 at Cornell High Energy Synchrotron Source, Cornell University, Ithaca, NY or beamline 24-ID at Advanced Photon Source, Argonne National Laboratories, Argonne, IL, for $Pa\_FleQ^{AAA\text{-}HTH}$-c-di-GMP). All diffraction images were processed using the software package XDS (47). The apo-$FleQ^{AAA}$ structure was solved using SAD with iodine as the anomalous scatterer, collected on crystals that were soaked in mother liquor supplemented with 500 mM NaI and 10% (vol/vol) ethylene glycol (48, 49). Initial phases were extended to 1.8 Å resolution from a native dataset using the PHENIX program package (50). ADP- and ATP-γ-S–bound Pa_FleQ^{AAA} were solved by molecular replacement in PHENIX, with the apo structure as the starting model. The structure of $Pa\_FleQ^{AAA\text{-}HTH}$–c-di-GMP was solved by SAD phasing with data collected on crystals grown from selenomethionine-derivatized protein. The heavy atom positions were determined with SHELX (51) and automatic building was conducted in PHENIX. For all constructs, iterative model building and refinement in COOT (52) and PHENIX yielded the final structural models.

Electron Microscopy. Pa_FleQ^{Full} (50 μM) was incubated with 100 μM ADP, 200 μM sodium vanadate, and 500 μM $MgCl_2$. Following a 30-min incubation on ice, the protein was gel-filtered against an ADP-vanadate–containing buffer [20 mM Tris·HCl pH 8.0, 100 mM NaCl, 2.5% (wt/vol) xylitol, 100 μM ADP, 200 μM sodium vanadate, and 500 μM $MgCl_2$] on a Superdex 200 10/300 GL size exclusion column (GE Healthcare). Five-microliter drops of protein at concentrations between 0.005 and 0.1 mg/mL were placed directly on glow-discharged carbon-coated grids (EMS) for 1 min. The grids were then blot-dried on filter paper and negatively stained with 2% (wt/vol) uranyl acetate in water. Specimens were examined on an FEI Tecnai T12 BioTWIN LaB6 electron microscope operating at 120 kV at nominal magnifications of 49,000 and 1–3 μm defocus. Images were recorded on a Gatan Ultrascan 4000 CCD camera. The contrast transfer function parameters were assessed using CTFFIND3 (53) and the phase flipping was done in SPIDER (54). Single particles were boxed manually and a single-particle stack was generated in EMAN2 (4,856 particles, 170 × 170-pixel box, 2.2 Å per pixel) (55). Normalization, centering, multireference alignment, multistatistical analysis, classification (~40 particles per class), and rotational autocorrelation function calculation were done in IMAGIC-4D (Image Science Software).

Isothermal Titration Calorimetry. Apparent dissociation constants (K_d) and stoichiometry of interaction (n) were measured by ITC using a VP-ITC calorimeter (Microcal). Calorimetric titrations of c-di-GMP (700 μM in the syringe; 7-μL injections) and wild-type or mutant Pa_FleQ^{Full} (30 μM in the cuvette) were carried out at 25 °C in assay buffer (25 mM Tris·HCl pH 8.0, 300 mM NaCl, 5 mM $MgCl_2$) with 150-s spacing between injections. ITC data were analyzed by integrating heat effects normalized to the amount of injected protein and curve-fitting based on a single-site binding model using the MicroCal Origin 7.0 software. Heat changes during ITC titrations likely combine contributions from c-di-GMP binding and accompanied changes in intra- and intermolecular protein interfaces. Heat from the dilution of c-di-GMP alone was subtracted before data analysis and the first injection was omitted from data processing.

In-Solution Chemical Cross-Linking. For oligomeric state detection, protein in cross-linking buffer (25 mM Hepes pH 8.0 and 300 mM NaCl) was incubated with EGS at room temperature. Protein and cross-linker concentrations and incubation times are specified in the respective figure legends. Cross-linking reactions were quenched by adding 50 mM Tris·HCl pH 8.0, followed by incubation at 97 °C for 10 min in standard SDS/PAGE sample buffer. Oligomer formation was analyzed by SDS/PAGE.

ATPase Activity Assay. ATPase activity of wild-type and mutant Pa_FleQ^{Full} was measured with the EnzChek Phosphate Assay kit (Life Technologies) (56). Assays were performed in triplicates in a 96-well plate according to the manufacturer's instructions. Briefly, ATPase reactions (200 μL; 1 μM enzyme) were carried in ATPase buffer (25 mM Hepes pH 8.0, 300 mM NaCl buffer, 1 mM DTT, 10 mM KCl, 1 mM $MgCl_2$, and 1 mM ATP). The reactions were monitored at 1-min intervals at 360 nm in a microplate reader.

***P. aeruginosa* Strain Construction, RNA Isolation, and Real-Time Quantitative PCR.** *P. aeruginosa* strains PAO1Δ*fleQ*Δ*fleN* or strains containing different mutations in the *fleQ* gene were routinely grown in LB medium at 37 °C. Mutations in the *fleQ* gene were generated by an overlapping PCR procedure. Briefly, PCR fragments containing the mutated *fleQ* gene and flanking genomic DNA were cloned into pEX19Gm or miniCTX2. $fleQ_{WT}$ and $fleQ_{R334E}$ were cloned into miniCTX2. $fleQ_{I374E}$, $fleQ_{V256E}$, $fleQ_{R185E}$, $fleQ_{V380E}$, and $fleQ_{T149E}$ were cloned into pEX19Gm. The resulting plasmids were then used to transform *E. coli* S17-1 strain and mobilized into the PAO1Δ*fleQ*Δ*fleN* strain. MiniCTX2 constructions allow the introduction of $fleQ_{WT}$ and $fleQ_{R334E}$ at the *attB* site on the *P. aeruginosa* chromosome, whereas pEX19Gm constructions allow the introduction of *fleQ* variant alleles at the *fleQ* native location. Plasmids pJN1120 (expressing YfiN/TpbB/PA1120 diguanylate cyclase) and pJN105 (empty vector) were electroporated into the constructed strains (14, 57, 58). Cell growth, RNA extraction, and RT-PCR were performed essentially as previously described (13, 14, 59). The *pelA*-forward (CCT TCA GCC ATC CGT TCT TCT) and *pelA*-reverse (TCG CGT ACG AAG TCG ACC TT) primers were used. Genomic DNA was used as a standard and transcript levels of all genes were normalized to total cDNA. Data presented are at least the average of two biological replicates. Error bars represent the SD between samples.

ACKNOWLEDGMENTS. We thank Rémi Fronzes for providing access to electron microscopy data collection and analysis software; and João Muniz and Raj Rajashankar for collecting diffraction data. Part of this work is based upon research conducted at the Cornell High Energy Synchrotron Source (CHESS), which is supported by the National Science Foundation (NSF) under award DMR-1332208, using the Macromolecular

Diffraction at CHESS (MacCHESS) facility, which is supported by award GM-103485 from the National Institute of General Medical Sciences, National Institutes of Health (NIH). The Northeastern Collaborative Access Team beamlines are funded by National Institute of General Medical Sciences/NIH under Award P41-GM103403. This research used resources of the Brazilian National Synchrotron Light Source (LNLS) and the Advanced Photon Source, a US Department of Energy Office of Science User Facility operated for the Department of Energy Office of Science by Argonne National Laboratory under Contract DE-AC02-06CH11357. P.V.K. is currently supported by the European Research Council. Our work was supported by Fundaçao de Amparo à Pesquisa do Estado de Sao Paulo under Grant 2009/13238-0 (to M.V.A.S.N.) and Fundaçao de Amparo à Pesquisa do Estado de Sao Paulo Fellowship 2011/24168-2 (to B.Y.M.); and by the NIH under Grants R01-AI097307 (to H.S.) and R01-GM56665 (to C.S.H.).

1. Hall-Stoodley L, Costerton JW, Stoodley P (2004) Bacterial biofilms: From the natural environment to infectious diseases. *Nat Rev Microbiol* 2(2):95–108.
2. Solano C, Echeverz M, Lasa I (2014) Biofilm dispersion and quorum sensing. *Curr Opin Microbiol* 18:96–104.
3. Srivastava D, Waters CM (2012) A tangled web: Regulatory connections between quorum sensing and cyclic Di-GMP. *J Bacteriol* 194(17):4485–4493.
4. Teschler JK, et al. (2015) Living in the matrix: Assembly and control of *Vibrio cholerae* biofilms. *Nat Rev Microbiol* 13(5):255–268.
5. Tolker-Nielsen T (2014) *Pseudomonas aeruginosa* biofilm infections: From molecular biofilm biology to new treatment possibilities. *APMIS Suppl* (138):1–51.
6. Furukawa S, Kuchma SL, O'Toole GA (2006) Keeping their options open: Acute versus persistent infections. *J Bacteriol* 188(4):1211–1217.
7. Mills E, Pultz IS, Kulasekara HD, Miller SI (2011) The bacterial second messenger c-di-GMP: Mechanisms of signalling. *Cell Microbiol* 13(8):1122–1129.
8. Römling U, Galperin MY, Gomelsky M (2013) Cyclic di-GMP: The first 25 years of a universal bacterial second messenger. *Microbiol Mol Biol Rev* 77(1):1–52.
9. Sondermann H, Shikuma NJ, Yildiz FH (2012) You've come a long way: c-di-GMP signaling. *Curr Opin Microbiol* 15(2):140–146.
10. Krasteva PV, Giglio KM, Sondermann H (2012) Sensing the messenger: The diverse ways that bacteria signal through c-di-GMP. *Protein Sci* 21(7):929–948.
11. Schirmer T, Jenal U (2009) Structural and mechanistic determinants of c-di-GMP signalling. *Nat Rev Microbiol* 7(10):724–735.
12. Arora SK, Ritchings BW, Almira EC, Lory S, Ramphal R (1997) A transcriptional activator, FleQ, regulates mucin adhesion and flagellar gene expression in *Pseudomonas aeruginosa* in a cascade manner. *J Bacteriol* 179(17):5574–5581.
13. Baraquet C, Murakami K, Parsek MR, Harwood CS (2012) The FleQ protein from *Pseudomonas aeruginosa* functions as both a repressor and an activator to control gene expression from the *pel* operon promoter in response to c-di-GMP. *Nucleic Acids Res* 40(15):7207–7218.
14. Hickman JW, Harwood CS (2008) Identification of FleQ from *Pseudomonas aeruginosa* as a c-di-GMP–responsive transcription factor. *Mol Microbiol* 69(2):376–389.
15. Ghosh T, Bose D, Zhang X (2010) Mechanisms for activating bacterial RNA polymerase. *FEMS Microbiol Rev* 34(5):611–627.
16. Gao R, Mack TR, Stock AM (2007) Bacterial response regulators: Versatile regulatory strategies from common domains. *Trends Biochem Sci* 32(5):225–234.
17. Gao R, Stock AM (2010) Molecular strategies for phosphorylation-mediated regulation of response regulator activity. *Curr Opin Microbiol* 13(2):160–167.
18. Bush M, Dixon R (2012) The role of bacterial enhancer binding proteins as specialized activators of σ54-dependent transcription. *Microbiol Mol Biol Rev* 76(3):497–529.
19. De Carlo S, et al. (2006) The structural basis for regulated assembly and function of the transcriptional activator NtrC. *Genes Dev* 20(11):1485–1495.
20. Lee SY, et al. (2003) Regulation of the transcriptional activator NtrC1: Structural studies of the regulatory and AAA+ ATPase domains. *Genes Dev* 17(20):2552–2563.
21. Baraquet C, Harwood CS (2013) Cyclic diguanosine monophosphate represses bacterial flagella synthesis by interacting with the Walker A motif of the enhancer-binding protein FleQ. *Proc Natl Acad Sci USA* 110(46):18478–18483.
22. Dasgupta N, Ramphal R (2001) Interaction of the antiactivator FleN with the transcriptional activator FleQ regulates flagellar number in *Pseudomonas aeruginosa*. *J Bacteriol* 183(22):6636–6644.
23. Jyot J, Dasgupta N, Ramphal R (2002) FleQ, the major flagellar gene regulator in *Pseudomonas aeruginosa*, binds to enhancer sites located either upstream or atypically downstream of the RpoN binding site. *J Bacteriol* 184(19):5251–5260.
24. Dasgupta N, et al. (2003) A four-tiered transcriptional regulatory circuit controls flagellar biogenesis in *Pseudomonas aeruginosa*. *Mol Microbiol* 50(3):809–824.
25. Dasgupta N, Arora SK, Ramphal R (2000) fleN, a gene that regulates flagellar number in *Pseudomonas aeruginosa*. *J Bacteriol* 182(2):357–364.
26. Srivastava D, Hsieh ML, Khataokar A, Neiditch MB, Waters CM (2013) Cyclic di-GMP inhibits *Vibrio cholerae* motility by repressing induction of transcription and inducing extracellular polysaccharide production. *Mol Microbiol* 90(6):1262–1276.
27. Dago AE, Wigneshweraraj SR, Buck M, Morett E (2007) A role for the conserved GAFTGA motif of AAA+ transcription activators in sensing promoter DNA conformation. *J Biol Chem* 282(2):1087–1097.
28. Wendler P, Ciniawsky S, Kock M, Kube S (2012) Structure and function of the AAA+ nucleotide binding pocket. *Biochim Biophys Acta* 1823(1):2–14.
29. Rappas M, et al. (2005) Structural insights into the activity of enhancer-binding proteins. *Science* 307(5717):1972–1975.
30. Zhang N, et al. (2014) Subunit dynamics and nucleotide-dependent asymmetry of an AAA(+) transcription complex. *J Mol Biol* 426(1):71–83.
31. Sysoeva TA, Chowdhury S, Guo L, Nixon BT (2013) Nucleotide-induced asymmetry within ATPase activator ring drives σ54-RNAP interaction and ATP hydrolysis. *Genes Dev* 27(22):2500–2511.
32. Su T, et al. (2015) The REC domain mediated dimerization is critical for FleQ from *Pseudomonas aeruginosa* to function as a c-di-GMP receptor and flagella gene regulator. *J Struct Biol* 192(1):1–13.
33. Chen C, et al. (2011) Representative proteomes: A stable, scalable and unbiased proteome set for sequence analysis and functional annotation. *PLoS One* 6(4):e18910.
34. Srivastava D, Harris RC, Waters CM (2011) Integration of cyclic di-GMP and quorum sensing in the control of vpsT and aphA in *Vibrio cholerae*. *J Bacteriol* 193(22): 6331–6341.
35. Trampari E, et al. (2015) Bacterial rotary export ATPases are allosterically regulated by the nucleotide second messenger cyclic-di-GMP. *J Biol Chem* 290(40):24470–24483.
36. Krissinel E (2015) Stock-based detection of protein oligomeric states in jsPISA. *Nucleic Acids Res* 43(W1):W314–W319.
37. Wigneshweraraj SR, et al. (2005) The second paradigm for activation of transcription. *Prog Nucleic Acid Res Mol Biol* 79:339–369.
38. Kulasakara H, et al. (2006) Analysis of *Pseudomonas aeruginosa* diguanylate cyclases and phosphodiesterases reveals a role for bis-(3′-5′)-cyclic-GMP in virulence. *Proc Natl Acad Sci USA* 103(8):2839–2844.
39. Malone JG, et al. (2010) YfiBNR mediates cyclic di-GMP dependent small colony variant formation and persistence in *Pseudomonas aeruginosa*. *PLoS Pathog* 6(3): e1000804.
40. Herrera MC, Krell T, Zhang X, Ramos JL (2009) PhhR binds to target sequences at different distances with respect to RNA polymerase in order to activate transcription. *J Mol Biol* 394(3):576–586.
41. Pittard J, Camakaris H, Yang J (2005) The TyrR regulon. *Mol Microbiol* 55(1):16–26.
42. Ueki T, Inouye S (2002) Transcriptional activation of a heat-shock gene, lonD, of *Myxococcus xanthus* by a two component histidine-aspartate phosphorelay system. *J Biol Chem* 277(8):6170–6177.
43. Andrews AE, Lawley B, Pittard AJ (1991) Mutational analysis of repression and activation of the tyrP gene in *Escherichia coli*. *J Bacteriol* 173(16):5068–5078.
44. Dixon MP, et al. (2002) The central domain of *Escherichia coli* TyrR is responsible for hexamerization associated with tyrosine-mediated repression of gene expression. *J Biol Chem* 277(26):23186–23192.
45. Wilson TJ, Maroudas P, Howlett GJ, Davidson BE (1994) Ligand-induced self-association of the *Escherichia coli* regulatory protein TyrR. *J Mol Biol* 238(3):309–318.
46. Yang J, et al. (2004) Mode of action of the TyrR protein: Repression and activation of the tyrP promoter of *Escherichia coli*. *Mol Microbiol* 52(1):243–256.
47. Kabsch W (2010) XDS. *Acta Crystallogr D Biol Crystallogr* 66(Pt 2):125–132.
48. Dauter Z, Dauter M, Rajashankar KR (2000) Novel approach to phasing proteins: Derivatization by short cryo-soaking with halides. *Acta Crystallogr D Biol Crystallogr* 56(Pt 2):232–237.
49. Nagem RA, et al. (2005) Getting the most out of X-ray home sources. *Acta Crystallogr D Biol Crystallogr* 61(Pt 8):1022–1030.
50. Adams PD, et al. (2010) PHENIX: a comprehensive Python-based system for macromolecular structure solution. *Acta Crystallogr D Biol Crystallogr* 66(Pt 2):213–221.
51. Sheldrick GM (2008) A short history of SHELX. *Acta Crystallogr A* 64(Pt 1):112–122.
52. Emsley P, Lohkamp B, Scott WG, Cowtan K (2010) Features and development of Coot. *Acta Crystallogr D Biol Crystallogr* 66(Pt 4):486–501.
53. Mindell JA, Grigorieff N (2003) Accurate determination of local defocus and specimen tilt in electron microscopy. *J Struct Biol* 142(3):334–347.
54. Shaikh TR, et al. (2008) SPIDER image processing for single-particle reconstruction of biological macromolecules from electron micrographs. *Nat Protoc* 3(12):1941–1974.
55. Tang G, et al. (2007) EMAN2: An extensible image processing suite for electron microscopy. *J Struct Biol* 157(1):38–46.
56. Webb MR (1992) A continuous spectrophotometric assay for inorganic phosphate and for measuring phosphate release kinetics in biological systems. *Proc Natl Acad Sci USA* 89(11):4884–4887.
57. Choi KH, Kumar A, Schweizer HP (2006) A 10-min method for preparation of highly electrocompetent *Pseudomonas aeruginosa* cells: Application for DNA fragment transfer between chromosomes and plasmid transformation. *J Microbiol Methods* 64(3):391–397.
58. Newman JR, Fuqua C (1999) Broad-host-range expression vectors that carry the L-arabinose-inducible *Escherichia coli* araBAD promoter and the araC regulator. *Gene* 227(2):197–203.
59. Schuster M, Lostroh CP, Ogi T, Greenberg EP (2003) Identification, timing, and signal specificity of *Pseudomonas aeruginosa* quorum-controlled genes: A transcriptome analysis. *J Bacteriol* 185(7):2066–2079.
60. Finn RD, et al. (2015) HMMER web server: 2015 update. *Nucleic Acids Res* 43(W1): W30–W38.
61. Wheeler TJ, Clements J, Finn RD (2014) Skylign: A tool for creating informative, interactive logos representing sequence alignments and profile hidden Markov models. *BMC Bioinformatics* 15:7.
62. Vidangos N, et al. (2013) Structure, function, and tethering of DNA-binding domains in σ(54) transcriptional activators. *Biopolymers* 99(12):1082–1096.

Supporting Information

Matsuyama et al. 10.1073/pnas.1523148113

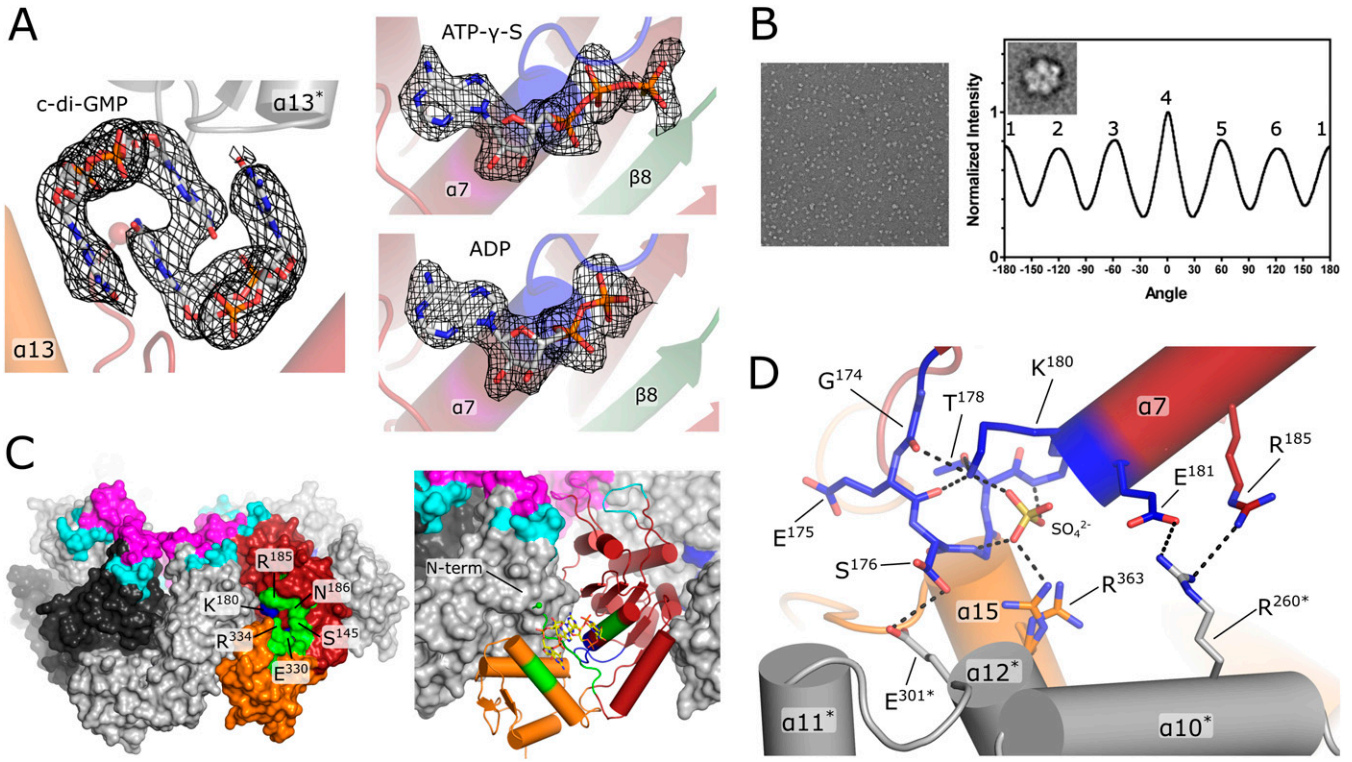

Fig. S1. Nucleotide binding and oligomerization of FleQ. (*A*) Crystallographic identification of ligands bound to the AAA+ domain of Pa_FleQ. Omit $|F_o| - |F_c|$ maps are contoured at 3.0 σ (black). The observed densities are consistent with the identity of the nucleotides used in cocrystallization trials [ATP-γ-S (*Right*, *Upper*), ADP (*Right*, *Lower*), c-di-GMP (*Left*)]. (*B*) Negative stain electron microscopy analysis of full-length *P. aeruginosa* FleQ. A typical micrograph showing single particles (*Left*) and an autorotation function of a class-average particle highlighting the sixfold auto-rotation axis (*Right*) are shown. Nominal magnification, *Left*: 49,000×, boxed particle class average: 170 × 170 pixels with a pixel size of 2.17 Å. (*C*) Accessibility of the c-di-GMP binding site in the context of a ring-shape AAA+ domain hexamer. Side views of a Pa_FleQ^{AAA} hexameric ring reconstructed from crystal symmetry are shown. Residues involved in c-di-GMP binding are colored green. Subdomains SD1 and SD2 of one protomer are colored as in Fig. 1; the other symmetry related protomers are colored in shades of gray. σ^{54} interaction loops L1 and L2 are presented in magenta and cyan, respectively. (*Right*) One of the protomers in a FleQ ring-shaped hexamer is shown in cartoon representation. The panel highlights that c-di-GMP-binding, as observed in the cocrystal structure, displaces the N-terminal tail of the AAA+ domain, which is incompatible with this ring-shaped oligomer form. (*D*) Role of Walker A residue K^{180} in FleQ AAA+ P-loop and hexameric ring stability. Residue K^{180} occupies a pivotal position for P-loop stabilization, interacting with the main-chain carbonyl oxygen of G^{174} and E^{175} and the side chain of T^{178}. Additionally, K^{180} is involved in the interaction network of the ADP/ATP-γ-S β–phosphate located at the N-terminal of helix α7 (the sulfate anion shown here occupies the nucleotide's β-phosphate position in the apo structure). Interactions between the side chains of S^{176} and E^{181} with E^{301} and R^{260} from neighboring protomers, respectively, contribute to hexameric ring formation.

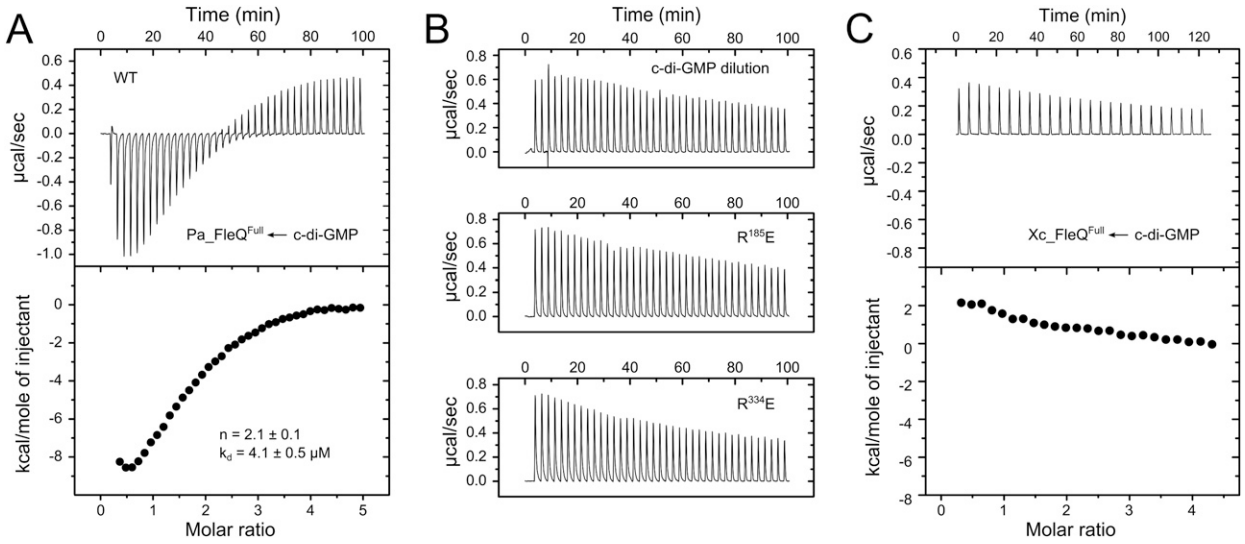

Fig. S2. ITC of full-length FleQ (Pa_FleQ^{Full} and Xc_FleQ^{Full}) with c-di-GMP. Wild-type protein or mutants with site-directed alteration in c-di-GMP binding residues, which were identified based on the cocrystal structure, are shown. (*A*) Titration of c-di-GMP to wild-type Pa_FleQ^{Full} shows a stoichiometry of 2:1 (c-di-GMP:FleQ) with a K_d of 4.1 μM. (*B*) Mutations $R^{185}E$ and $R^{334}E$ completely abolish ligand binding, as evidenced by the endothermic peak profiles that are similar to those observed by c-di-GMP dilution into buffer (*Upper*). Wild-type Pa_FleQ^{Full} data were reproduced in Fig. 4 for comparison with other site-directed mutant proteins. (*C*) Titration of c-di-GMP to wild-type, full-length *Xanthomonas citri* FleQ (Xc_FleQ^{Full}).

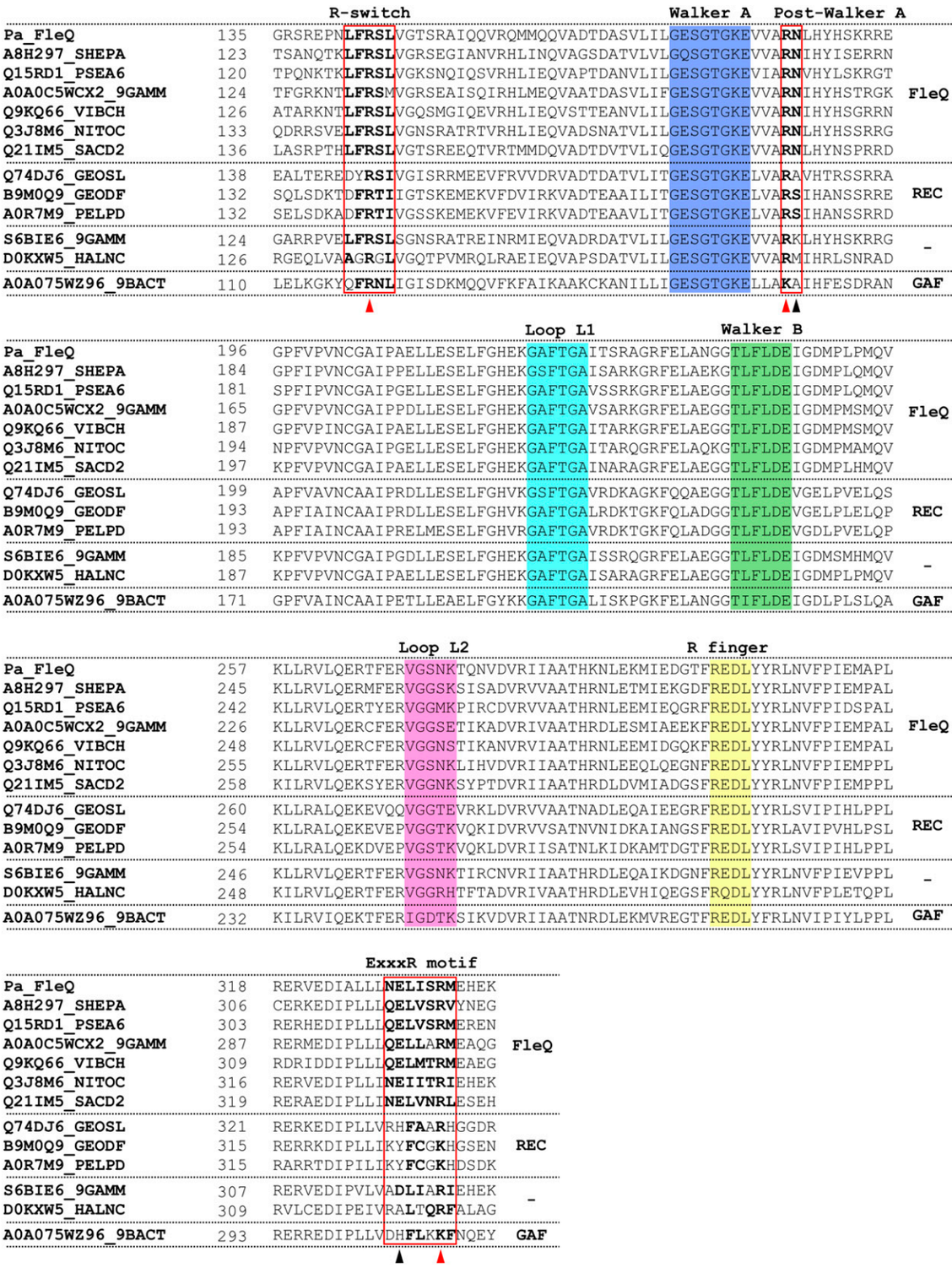

Fig. S3. Alignment of representative bEBPs with putative c-di-GMP binding site. The alignment was generated with representative sequences from Table 1 and Table S2. Coloring of conserved features (Walker A, Walker B, Loop L1, Loop L2, and R finger) follows the same scheme as introduced in Fig. 1*A*. C-di-GMP binding motifs are highlighted in red boxes, conserved residues (compared with Pa_FleQ) in these motifs are in bold. Red arrowheads below the alignment point to conserved arginine (or lysine) residues that coincide with arginine residues in FleQ important for c-di-GMP binding. Black arrowheads mark other c-di-GMP–interacting residues identified in the structure. Dashed lines separate sequences by nature of their N-terminal domain as in Table 1 [FleQ-like, REC, GAF, and without recognizable N-terminal domains (-), indicated in the right column]. The first and second column list Uniprot identifiers and residue numbering, respectively. The following sequences were used: A8H297_SHEPA: *Shewanella pealeana* (*strain ATCC 700345/ANG-SQ1*); Q15RD1_PSEA6: *Pseudoalteromonas atlantica* (strain T6c/ATCC BAA-1087); A0A0C5WCX2_9GAMM: *Photobacterium gaetbulicola Gung47*; Q9KQ66_VIBCH: *Vibrio cholerae serotype O1* (strain ATCC 39315/EI Tor Inaba N16961); Q3J8M6_NITOC: *Nitrosococcus oceani* (strain ATCC 19707/NCIMB 11848); Q21IM5_SACD2: *Saccharophagus degradans* (strain 2–40/ATCC 43961/DSM 17024); Q74DJ6_GEOSL: *Geobacter sulfurreducens* (strain ATCC 51573/DSM 12127/PCA); B9M0Q9_GEODF: *Geobacter daltonii* (strain DSM 22248/JCM 15807/FRC-32); A0R7M9_PELPD: *Pelobacter propionicus* (strain DSM 2379); S6BIE6_9GAMM: endosymbiont of unidentified scaly snail isolate Monju; D0KXW5_HALNC: *Halothiobacillus neapolitanus* (strain ATCC 23641/c2) (*Thiobacillus neapolitanus*); A0A075WZ96_9BACT: *Thermodesulfobacterium commune* DSM 2178.

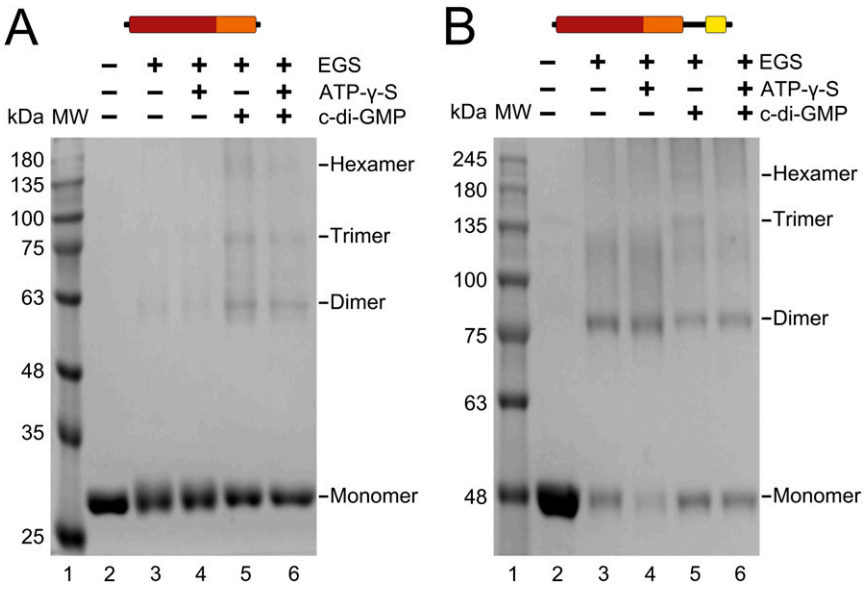

Fig. S4. Cross-linking analysis of Pa_FleQ^{AAA} and Pa_FleQ$^{AAA\text{-}HTH}$ oligomerization in solution. SDS/PAGE of Pa_FleQ^{AAA} (*A*) and Pa_FleQ$^{AAA\text{-}HTH}$ (*B*) proteins (10 μM) incubated with the primary amine-specific cross-linker EGS (1 mM) for 30 min at room temperature are shown. Addition of nucleotides (100 μM) is indicated above the gel. Calculated monomer molecular weights: Pa_FleQ^{AAA}, 29.1 kDa; Pa_FleQ$^{AAA\text{-}HTH}$, 38.2 kDa. Migration pattern of probable oligomeric species are indicated on the right of each gel. Diagrams above each gel depict the domain architecture of the constructs used in each experiment.

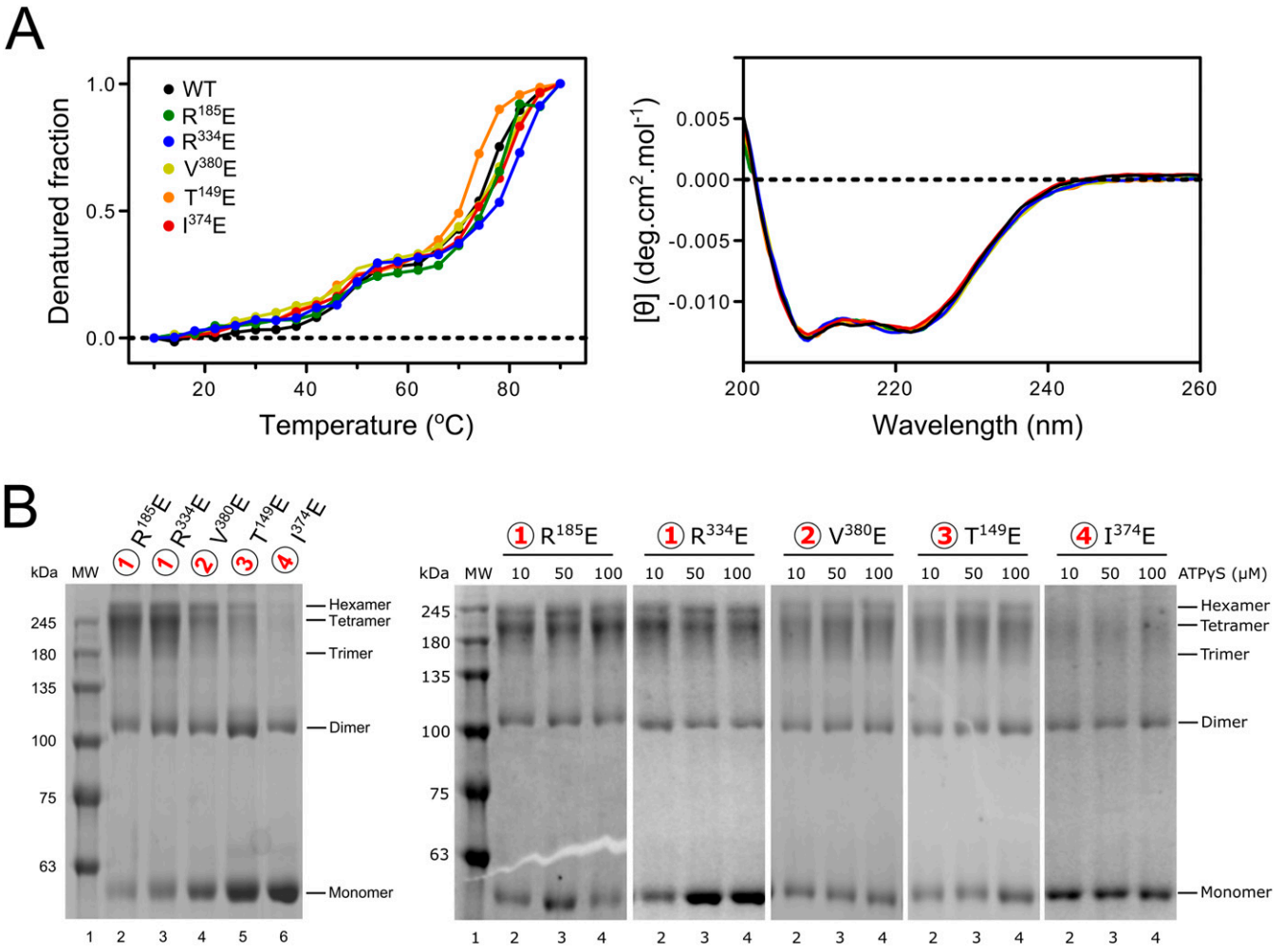

Fig. S5. Thermal stability and cross-linking analyses of Pa_FleQ^{Full} variants. (*A*) Protein stability. Thermal unfolding of full-length FleQ variants was monitored by plotting the intensity of the circular dichroism signal at 222 nm upon heat denaturation. Curves are plotted as fraction of completely denatured protein (90 °C). Ellipticity (θ) scans over a wavelength range of 200–260 nm at 20 °C are shown for all samples (*Right*). (*B*) Cross-linking analyses of Pa_FleQ^{Full} mutant variants. The impact of c-di-GMP (50 μM; *Left*) and increasing concentration of ATP-γ-S (10–100 μM; *Right*) on the oligomerization of Pa_FleQ^{Full} mutants (50 μM) was monitored by EGS-mediated cross-linking. Reactions were carried out in reaction buffer containing 250 μM EGS at room temperature for 30 min.

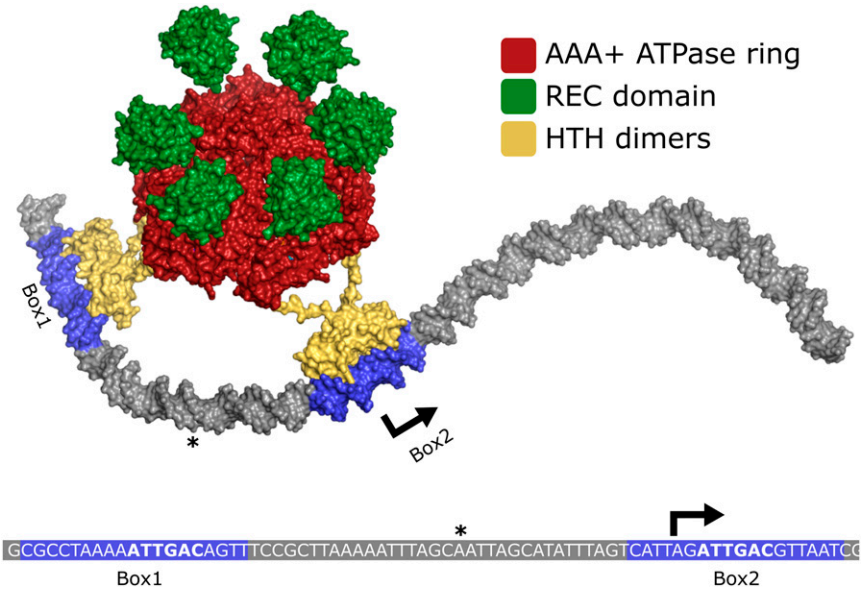

Fig. S6. Model of full-length Pa_FleQ hexameric rings bound to *pel* promoter DNA. A full-length FleQ model was generated by combining the crystal structure of a Pa_FleQ^{AAA} hexameric ring with the REC and HTH domain models based on PDB ID codes 1NY5 and 4L5E, respectively (20, 62). The position of the REC and HTH domains were guided by the position of the N- and C-termini of FleQ^{AAA} protomers. A stretch of DNA with FleQ boxes 1 and 2 was modeled as well, with the sequence of the *pel* promoter shown below. The asterisk indicates the position of the hypersensitive site identified by DNase I footprinting experiments (13).

Table S1. Data collection and refinement statistics

Data collection and refinement	Pa_FleQ^{AAA} NaI derivative	Pa_FleQ^{AAA}	Pa_FleQ^{AAA}+ ADP	Pa_FleQ^{AAA}+ ATP-γ-S	Pa_FleQ$^{AAA\text{-}HTH}$ + c-di-GMP
Data collection					
Wavelength (Å)	1.4592	1.4592	1.4592	1.5418	0.9792
Space group	$P6_5$	$P6_5$	$P6_5$	$P6_5$	$P6_322$
Unit cell (Å)	104.3, 104.3, 43.6, 90°, 90°, 120°	104.9, 104.9, 42.7, 90°, 90°, 120°	104.9, 104.9, 42.7, 90°, 90°, 120°	105.3, 105.3, 42.9, 90°, 90°, 120°	137.9, 137.9, 172.8, 90°, 90°, 120°
Resolution range (Å)	34.1–2.0 (2.1–2.0)	45.4–1.8 (1.9–1.8)	45.4–2.4 (2.6–2.4)	52.6–2.5 (2.6–2.5)	43.6–3.3 (3.6–3.3)
Total reflections	171,250 (26,903)	261,119 (40,636)	130,070 (15,867)	73,821 (6,398)	131,292 (3,251)
Unique reflections	35,716 (5,693)	25,124 (4,007)	10,840 (1,719)	9,612 (1,042)	24,350 (650)
Completeness (%)	99.2 (98.0)	99.5 (98.8)	99.9 (99.4)	99.9 (99.5)	88.5 (47,8)
Redundancy	4.8 (4.7)	10.4 (10.1)	12.0 (9.2)	7.7 (6.1)	5.4 (5.0)
I/σ (I)	10.2 (2.0)	14.7 (2.6)	16.3 (2.0)	6.1 (1.8)	17.9 (1.8)
R-meas (%)	12.8 (92.1)	13.8 (97)	15.5 (126.5)	16.6 (55.4)	8.5 (71.5)
Refinement					
R-work (%)		16.8	18.1	17.8	26.3
R-free (%)		21.0	25.2	22.9	29.0
Number of atoms					
Protein		2,029	2,022	1,995	2,028
Nucleotide		—	27	31	92
Water		268	81	148	0
Average B-factor					
Protein		21.5	40.2	21.6	92.1
Nucleotide		—	29.7	24.4	39.6
Water		33.1	38.8	22.5	0
RMSD					
Bonds (Å)		0.007	0.007	0.009	0.013
Angles (°)		1.004	1.144	1.195	2.536
Ramachandran (%)					
Favorable		98.4	95.6	98.0	85.1
Allowed		1.6	4.0	2.0	11.4
Outliers		0.0	0.4	0.0	3.5

Statistics for high-resolution shell are shown in parentheses.

Table S2. bEBPs predicted to contain a conserved c-di-GMP binding motif (sequences associated with Table 1, column 3)

FleQ domain		GAF domain		No N-terminal domain		REC domain	
Accession	Organism	Accession	Organism	Accession	Organism	Accession	Organism
Q0AAS7	*Alkalilimnicola ehrlichii*	Q6NA12	*Rhodopseudomonas palustris*	S6BIE6	unclassified	B5EAE4	*Geobacter bemidjiensis*
Q8ECB1	*Shewanella oneidensis*	H9U.K.K9	*Spirochaeta africana*	W0TKX7	*Thiolapillus brandeum*	E6VV23	*Desulfovibrio aespoeensis*
K4KHP1	*Simiduia agarivorans*	F8F1U5	*Treponema caldarium*	D0KXW5	*Halothiobacillus neapolitanus*	F6B7S3	*Desulfotomaculum carboxydivorans*
A0A0C5WCX2	*Photobacterium gaetbulicola*	A0A075WZ96	*Thermodesulfobacterium commune*	A4A600	*Congregibacter litoralis*	D3FVN4	*Bacillus pseudofirmus*
Q9KQ66	*Vibrio cholerae*	B3DZA5	*Methylacidiphilum infernorum*	Q31FN5	*Thiomicrospira crunogena*	I8RAD9	*Pelosinus fermentans*
W8L6B7	*Halorhodospira halochloris*			D3RRD4	*Allochromatium vinosum*	C6BU16	*Desulfovibrio salexigens*
D4ZIA0	*Shewanella violacea*			I3Y607	*Thiocystis violascens*	F8A837	*Thermodesulfatator indicus*
A3QCN3	*Shewanella loihica*			D3S9F9	*Thioalkalivibrio sp.*	F2NE61	*Desulfobacca acetoxidans*
Q12PM0	*Shewanella denitrificans*					B5EBB4	*Geobacter bemidjiensis*
B1KLH5	*Shewanella woodyi*					A5GDQ0	*Geobacter uraniireducens*
B8GT39	*Thioalkalivibrio sulfidiphilus*					C8W398	*Desulfotomaculum acetoxidans*
F2G3X6	*Alteromonas macleodii*					A0A075WYK6	*Thermodesulfobacterium commune*
A1WUC6	*Halorhodospira halophila*					A7IE40	*Xanthobacter autotrophicus*
Q7MIN1	*Vibrio vulnificus*					E1WYR5	*Halobacteriovorax marinus*
Q085N4	*Shewanella frigidimarina*					F6CNR7	*Desulfotomaculum kuznetsovii*
Q3J8M6	*Nitrosococcus oceani*					A4J4N7	*Desulfotomaculum reducens*
Q21IM5	*Saccharophagus degradans*					A4J616	*Desulfotomaculum reducens*
E1VPK4	*Gamma proteobacterium HdN1*					F8ABW9	*Thermodesulfatator indicus*
C1DQF1	*Azotobacter vinelandii*					B8FJT8	*Desulfatibacillum alkenivorans*
C5BRZ8	*Teredinibacter turnerae*					Q6MHV3	*Bdellovibrio bacteriovorus*
B3PEX8	*Cellvibrio japonicus*					D8PFF7	*Nitrospira defluvii*
A0A0C5VAJ5	*Gynuella sunshinyii*					W5X1M1	*Bdellovibrio bacteriovorus*
R4YT01	*Oleispira antarctica*					A8MGT2	*Alkaliphilus oremlandii*
U4K2L0	*Vibrio nigripulchritudo*					F6B3K1	*Desulfotomaculum carboxydivorans*
A0A098G2Y6	*Legionella fallonii*					M4VEB7	*Bdellovibrio exovorus*
F7YNB5	*Vibrio anguillarum*					F6DU39	*Desulfotomaculum ruminis*
Q87MJ6	*Vibrio parahaemolyticus*					Q39XH0	*Geobacter metallireducens*
F0LV23	*Vibrio furnissii*					C8WYS9	*Desulfohalobium retbaense*
I1XLA6	*Methylophaga nitratireducenticrescens*					Q3A223	*Pelobacter carbinolicus*
D3HJ18	*Legionella longbeachae*					Q2IMP6	*Anaeromyxobacter dehalogenans*
Q5ZX79	*Legionella pneumophila*					I0GJJ1	*Caldisericum exile*
G3XCV0	*Pseudomonas aeruginosa*					A0A075K6I7	*Pelosinus sp.*
K0WPZ8	*Pseudomonas fluorescens*					Q3B5Z9	*Chlorobium luteolum*
A0A089ZPQ9	*Pseudomonas rhizosphaerae*					I4D1F0	*Desulfosporosinus acidiphilus*
L0GTK0	*Thioflavicoccus mobilis*					Q2IHE3	*Anaeromyxobacter dehalogenans*
Q4KG73	*Pseudomonas fluorescens*					Q39XK6	*Geobacter metallireducens*
Q485M5	*Colwellia psychrerythraea*					C7PEX2	*Chitinophaga pinensis*
A0A077LJ97	*Pseudomonas sp.*					Q74DJ6	*Geobacter sulfurreducens*
K0C4W0	*Cycloclasticus sp.*					Q1MQI6	*Lawsonia intracellularis*
G4QLX6	*Glaciecola nitratireducens*					A7HIM1	*Anaeromyxobacter sp.*
A0A089WSC4	*Pseudomonas cremoricolorata*					M1WKA5	*Desulfovibrio piezophilus*
G8Q0L8	*Pseudomonas fluorescens*					Q3A356	*Pelobacter carbinolicus*

Table S2. Cont.

FleQ domain		GAF domain		No N-terminal domain		REC domain	
Accession	Organism	Accession	Organism	Accession	Organism	Accession	Organism
E1SUP9	*Ferrimonas balearica*					B9M0Q9	*Geobacter daltonii*
A0A097QM59	*Vibrio coralliilyticus*					J7IP96	*Desulfosporosinus meridiei*
A4VMJ3	*Pseudomonas stutzeri*					A0R7M9	*Pelobacter propionicus*
Q884Y2	*Pseudomonas syringae*					H1XQY8	*Caldithrix abyssi*
A1U263	*Marinobacter hydrocarbonoclasticus*					A6TT75	*Alkaliphilus metalliredigens*
W8RVQ1	*Pseudomonas stutzeri*					Q39VU3	*Geobacter metallireducens*
Q2SBU8	*Hahella chejuensis*					F3Z0Y5	*Desulfovibrio africanus*
A0A098GFT6	*Tatlockia micdadei*					D0LFQ8	*Haliangium ochraceum*
I1YKN4	*Methylophaga frappieri*					C8W392	*Desulfotomaculum acetoxidans*
D5BV80	*Nitrosococcus halophilus*					E8RDW7	*Desulfobulbus propionicus*
F9T4M1	*Vibrio tubiashii*					D6Z2J3	*Desulfurivibrio alkaliphilus*
B7VL01	*Vibrio tasmaniensis*					F0JC51	*Desulfovibrio desulfuricans*
Q6LTP6	*Photobacterium profundum*					G7W595	*Desulfosporosinus orientis*
Q5E3P5	*Vibrio fischeri*					Q2LSK2	*Syntrophus aciditrophicus*
A0A0A8UN75	*Legionella hackeliae*					D3PA19	*Deferribacter desulfuricans*
A1S800	*Shewanella amazonensis*					B3E969	*Geobacter lovleyi*
M5E625	*Thalassolituus oleivorans*					A0LPT2	*Syntrophobacter fumaroxidans*
A8H297	*Shewanella pealeana*					D5MM35	*Candidatus Methylomirabilis oxyfera*
Q15RD1	*Pseudoalteromonas atlantica*					I0AG67	*Ignavibacterium album*
A0A024HES6	*Pseudomonas knackmussii*					A5GFK3	*Geobacter uraniireducens*
Q88ET0	*Pseudomonas putida*						
F6A8I2	*Pseudomonas fulva*						
S6AU94	*Pseudomonas resinovorans*						
A4XW68	*Pseudomonas mendocina*						
C3K0U9	*Pseudomonas fluorescens*						